Multiscale Simulation of Fluids: Coupling Molecular and Continuum

Edward R. Smith[*a] and Panagiotis E. Theodorakis[*b]

Computer simulation is an important tool for scientific progress, especially when lab experiments are either extremely costly and difficult or lack the required resolution. However, all of the simulation methods come with limitations. In molecular dynamics (MD) simulation, the length and time scales that can be captured are limited, while computational fluid dynamics (CFD) methods are built on a range of assumptions, from the continuum hypothesis itself, to a variety of closure assumptions. To address these issues, the coupling of different methodologies provides a way to retain the best of both methods. Here, we provide a perspective on multiscale simulation based on the coupling of MD and CFD with each a distinct part of the simulation domain. This style of coupling allows molecular detail to be present only where it is needed, so CFD can model larger scales than possible with MD alone. We present a unified perspective of the literature, showing the links between state and flux coupling and discuss the various assumptions required for both. A unique challenge in such coupled simulation is obtaining averages and constraining local parts of a molecular simulation. We highlight that incorrect localisation has resulted in an error in the literature for both pressure tensor and coupling constraints. We then finish with some applications, focused on the simulation of fluids. Thus, we hope to motivate further research in this exciting area with applications across the spectrum of scientific disciplines.

Technological advancements in computer software and hardware, combined with scientific ingenuity has led to the development of a wealth of novel computational methodologies over the years. This has established computer simulation as a key tool in a wide spectrum of fields in science and engineering across academia and industry. Moreover, the implementation of simulation techniques is often provided as open-source or free software, which allows for the widespread use of the methods in various applications, accelerating software development, and facilitating scientific exchange, validation, and eventually progress. As a result, unprecedented perspectives in scientific research unfold, with simulation already having a leading role in the study of physical and chemical processes, and novel materials' design. This is important since simulation can offer advantages in cases that lab experiments are costly, difficult, dangerous, lack the necessary resolution or are simply impossible.

Luckily, a number of well-established simulation methods supported by open-source or free software are available to scientists nowadays. However, each simulation method is only suitable for capturing a particular range of length and time scales of a phe-nomenon. For example, at the scale of most engineering problems, the continuum assumptions allow a fluid to be described using partial differential equations. These equations require a number of assumptions to model fluids, such as a constant viscosity coefficient[1], a sharp interface with well-defined surface tension[2] or a simple relationship between angle and movement of a contact line[3], which can be shown to break down at small enough scales. At these small scales, molecular dynamics (MD) simulation is able to describe the wider range of physics required. However, MD is limited to systems in nanometre length scales and nanosecond time scales. With fit-for-purpose hardware and software, MD has been applied in systems of up to 2 billion particles[4] or second time scales.[5] This is still well short of the 10^{25} molecules present in a single m^3 of air and, barring a revolution in computing power, will remain unsuitable for problems beyond the microscale. Hence, it is very much desirable to invent new simulation protocols that will be able to combine a multitude of distinct methods under the same hood (single simulation), thus coherently providing a detailed description of the system's behaviour across scales. In turn, this might allow for a better understanding of the studied phenomena. The coupling of simulation methods that share time and length scales allows information to be easily transferred from one simulation technique/domain to the other. This guarantees a well-defined 'interface' between the two methods/domains. The basis of this method is the exchange of quanti-

---

[b] Department of Mechanical and Aerospace Engineering, Brunel University London, Uxbridge, Middlesex UB8 3PH, UK; E-mail: Edward.Smith@brunel.ac.uk

[a] Institute of Physics, Polish Academy of Sciences, Al. Lotników 32/46, 02-668 Warsaw, Poland; E-mail: panos@ifpan.edu.pl

ties between the continuum and the MD domain during the simulation using constraints and averaging to guarantee consistency at the interface.

In this perspective article, we aim to provide a discussion on the current status and outlook of coupled simulation approaches with a focus on the area of fluid dynamics. Of particular interest is the theoretical underpinnings of coupled MD–continuum modelling in fluids with domain decomposition. Some examples of application areas are also given. Therefore, this does not aim to be a thorough review of the literature for every single simulation method, there have been a wide range of reviews. [6–12]. We also do not aim to discuss aspects, such as the creation of coarse-grained models from bottom-up approaches (*e.g.* iterative Boltzmann inversion methods, free energy methods, *etc.* [13]), or the coupling of simulation methods with experimental data. [14] Nor is it a discussion of the combination of different force-fields in the same simulation method (*e.g.* MD as in the case of GōEN [15] and GōMARTINI models [16]) used in fields, such as biophysics. [17,18]

Instead, the focus here is on the development of the theoretical coupling methods that have matured over the years. In a 2006 report anticipating the world beyond 2020, multi-scale modelling is imagined to be foundational for many emerging technologies, shaping the future of research. [19] This was inspired by quantum to classical coupling using MD, important to the 2013 Nobel Prize awarded to Arieh Warshe, Michael Levitt, and Martin Karplus (a brief overview of these methods will be given in Section 1). However, in many ways the coupling of molecular to continuum systems for fluid dynamics have not taken off in the same way. Fluid coupling models remain in their infancy and very few industrial success stories using multi-scale linked simulations that incorporate molecular detail have been put out. Perhaps a major factor is the tragic loss of two pioneers and champions in multiscale modelling, first Jason Reese in 2019 at only 51 then Mark Robbins in 2020 at 64. The effect on both the scientific community and the research funding landscape is profound. In addition, coupled simulation has never become mainstream in the fluid dynamics community, suffering from a combination of implementational complexity and limited or niche areas of application. This potential challenge was identified back in 2006 by Ref. 19 underlining the overwhelming software complexity requiring 'industrial-scale' and industry-wide support. A limitation also acknowledged succinctly in Tong *et al.* [11], *It is the time to introduce the multi-scale methods, especially the "coupling methods", to the applications on more practical multiscale heat transfer and fluid flow problems. Both the fundamental and practical researches will benefit from this applications, and the multiscale simulations will have a promising future.* A recent review of multiscale modelling for nanofluids [12] suggests further development and improvement are required before these methods can be applied to the study of nanofluidics.

The state of the literature is summarised by Tong *et al.* [11], paraphrasing Fish that *"most new technologies began with a native euphoria"* when the inventions were overpromised. *The rapid development led to a "peak of hype" and followed by a period of crash when the immaturity of the ideas was overreacted.* This can be seen graphically in Fig. 1 where the literature on domain decomposition coupling is shown superimposed on a Gartner hype
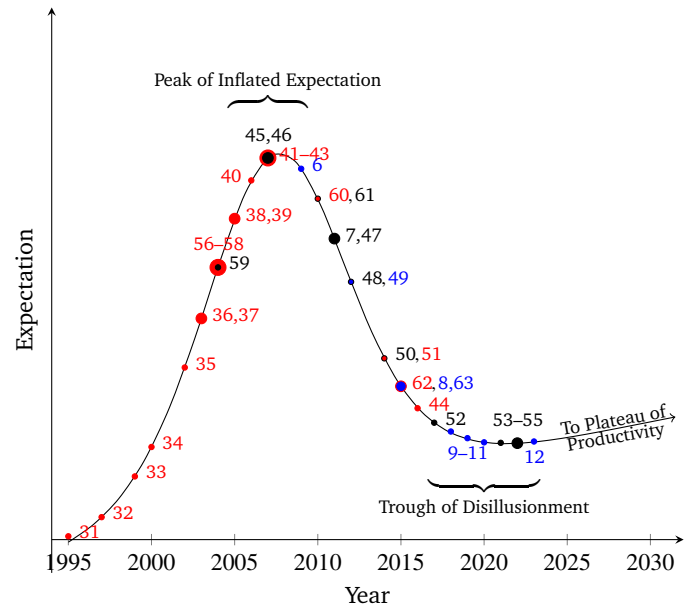

Fig. 1 The literature on domain decomposition coupling as a function of time shown on the Gartner hyper cycle, [20] a model for the growth of new technologies where the expectations of a technology over time show a peak followed by a trough. The theoretical contributions are shown in red, the applications in black, and the review articles are shown in blue.

cycle [20]. Although a fairly arbitrary model for the adoption of a new technology, it provides a useful perspective on the development of coupling technology. The literature is coloured by papers developing theory or methods (in red), papers applying coupling to problems (black) or publications which review or provide perspectives on coupling (blue). After a wave of literature developing the method, expectations reach a peak followed by a period where the important applications and industrial adoption are slow to catch up. Recent years see a large number of review articles, which characterise the evocatively titled 'trough of disillusionment', but with some impressive applications starting to appear. The lack of methodological development (points in red) is also clear after the peak on Fig 1. It is for this reason the current perspective focuses on unifying the literature in order to establish a framework to continue development of the theory to handle the cases needed for increased industrial adoption. In this perspective we set out the state of the art in theoretical development, before listing the recent applications which demonstrate the coupling method, in the hope it can lead the field to the 'plateau of productivity'. Although a large factor in getting to productivity is the software for coupling, this will not be detailed here and have been omitted from Fig 1. A range of coupling software exists, which can be divided into monolithic [21], frameworks [22,23] and libraries [24–26]. Many of these types of coupling models are summarised in various published reviews [27–29] including previous work by the authors. [30] Instead we focus on the theoretical aspects of the problem.

There are a disparate range of methodologies for domain decomposition coupling, often with researchers working using a preferred model. With this in mind, we focus in this perspective on trying to present a unified framework which can link together

various models applied throughout the literature. We show the similarity between the different approaches, and provide a rigorous underpinning to unify the literature and provide a tool to enable new theoretical developments.

Through our discussion, we aim to lower the barrier for embarking on hybrid multiscale computer simulations. The rapidly evolving field of machine learning for fluids looks set to provide promising ways of course-graining and coupling through data-driven approximation of underlying physical processes. However, such data driven machine learning methods cannot replace the theoretical development of schemes which respect conservation laws, as focused on in this perspective. Moreover, such mathematical forms for coupled conservation laws are likely to be essential ingredients to build constraints into physics-inspired neural network[64]. This is particularly important, as building the new generation of powerful coupled (hybrid) simulation methods and exploiting the increasing capabilities in software and hardware requires scientists with broader computational and scientific skills and creativity, based on a deeper knowledge of multiple simulation methodologies across scientific fields. Thus, our perspective article also provides opportunities for experts that are thinking of exploring the capabilities of hybrid simulation schemes in their research areas.

1 Brief Perspective on Other Coupling Approaches

1.1 *Ab initio* Molecular Dynamics

Ab initio MD methods belong to this category of coupled simulation approaches. Here, classical examples are the Born–Oppenheimer MD, the Ehrenfest MD, and the Car–Parrinello MD (CPMD) methods.[65,66] The goal of these methods is to enhance the capability of MD in describing processes that depend on the electronic degrees of freedom and, also, better describe many-body effects. From the perspective of quantum methods the use of MD enables a faster evolution of the nuclear positions, based on empirical interactions. The aim of *ab initio* MD is to carry out the classical dynamics of nuclei and use a quantum dynamics approach for electrons. Among the *ab initio* MD methods, the most prominent is probably Car–Parrinello MD (CPMD), since it allows for larger time steps in the classical approach and avoids solving the electronic structure problem at each time. The method has been well-established over the years with further developments that include its application in various statistical ensembles. The electronic degrees of freedom are introduced into the model as additional degrees of freedom as part of an extended Lagrangian equation of motion, which evolves both the ionic and electronic degrees of freedom. As an advantage, CPMD does not require matrix diagonalisation, as in the case of the Born–Oppenheimer MD, and electrons are assumed to be in the electronic ground state (adiabatic approximation) during the motion of the ions (nuclei). The application of the CPMD method in fluids includes mainly examples such as the proton transport in bulk water.[67] Research in this area is active and new developments are expected to enable larger time and length scales while at the same time holding the capabilities of describing the electronic state of a system, which would allow for the study of more complex phenomena, especially those relying on charge interactions. *Ab initio* MD simulations are still more focused on material design (structure and properties, including electronic properties), rather than fluid dynamics problems that require the simulation of flow changes or even heat transfer. However, subjects such as tribology require a detailed model of the fluid and solid material with some interface interactions dependant on the *Ab initio* detail.[68] As computing capabilities continuously increase, a wider range of applications in fluid dynamics might start to employ *ab initio MD* methods in the future. These might be used to parametrise intermolecular interactions at these interfaces for use in classical solvers, or applied directly in coupled QM–MM methods as described in the next subsection 1.2.

1.2 Coupling Quantum–Molecular Mechanics

While in the case of *ab initio* MD methods the classical and electronic degrees of freedom are attempted to be solved together, for example, based on an extended Lagrangian of motion,[66] a more common strategy is to use methods with different resolution for different parts of the system and establish the interface region between the methods. In this category of coupling fall quantum mechanics/molecular mechanics (QMMM) methods,[69] which have been very popular in investigating biological systems.[70] Here, a part of the system is treated classically, while another part that is of particular interest for a process is simulated quantum-mechanically. The classical approach usually refers to molecular-mechanics (MM) simulations, which include a detailed description of the system, that is, all atoms are explicitly modelled, angle and dihedral-angle potentials, point charges, *etc.*. A focus of this method is to establish accurate descriptions of the interactions between the QM and the MM systems, especially for situations of covalently bonded atoms and electrostatic QMMM interactions, or when particles are moving between the QM and the MM domains. Various approaches trying to address these issues have been considered, with this area being under intensive development, for example, through various embedding methods, such as mechanical, electrostatic and polarised, and boundary schemes, such as link atom, boundary atom, and localised-orbital schemes. A common approach for QMMM simulations is ONIOM,[71] which is available in most popular open-source MD softwares with a focus on biological systems. However, most simulations in fluid dynamics do not require the focus on the nature of such properties and such methods are less used in fluids. Still, as we manage to gain greater ability to describe the properties and structure of fluids and simulate ever larger systems, the ability of obtaining electronic structure information can emerge as an asset in the future, especially in micro-chip technologies. Efforts to couple various methods in this area also remain in the focus of simulation, such as the recent effort to couple Density Functional Theory with Dynamical Mean Field Theory within the Framework of Linear Combination of Numerical Atomic Orbitals.[72] It will be interesting to couple such methods with larger time- and length-scale resolutions in the case of fluids simulation. In tribological applications, such coupled methods have recently been applied to model shear and boundary lubrication where reactions would

be expected to occur.[73] Finally, method developments in the coupling of QM and MM domains can provide a basin of ideas for the molecular–continuum coupling, which is important in fluid dynamics phenomena and will be discussed in more detail later.

1.3 Coupling Molecular-Molecular and Molecular-Mesoscale

There are a range of cases where the coupling between discrete methods can be beneficial. For example, coupling Monte Carlo (MC) and MD methods can take place for both all-atom and coarse-grained models, and at the molecular and mesoscale level. The method can be implemented as a multistep approach[74] or within the single simulation in cycles of MC and MD,[75] where MC can refer to a range of different methods, *e.g.* Wang–Landau.[76] Since both methods are particle-based in the context of fluids and the same force-field is used (unless coupling takes place at the level of model description, as, for example, in the case of AdResS[77,78]), the coupling is mainly of a technical nature. In this approach, the advantages of both methods are exploited in the same simulation. On the one hand, in the case of MC a large selection of potential moves are available to facilitate larger conformation changes of the system and the exploration of the phase space of the system including complex moves which would be unlikely to occur even in long MD runs. Moreover, MC offers the advantage of directly sampling the energy of a system. On the other hand, in the case of MD the dynamics can be obtained as a function of time, and the molecular velocities are available for each system snapshot. In addition, MD is a method that is easy to scale on massively parallel computing architectures. One aspect that requires consideration is differences related to the concept of time in the two methods, as the time in MC is something that can be only indirectly defined, for example, through diffusion. Regarding applications of MC–MD schemes in fluids, the approach has been particularly useful in soft matter systems with complex molecules and open-source software is generally available, which can combine MD and MC in various ensembles.[79] An increase in the computational efficiency has been noted when configurational bias is included in the MC scheme. Typically, such simulations can be beneficial for simulation of molecules, for example regarding the hydration of a buried binding pocket in bovine pancreatic trypsin inhibitor.[79] Although different bias can be included in both the MD and the MC approaches, MC allows for a greater flexibility since MD requires a more careful treatment of the system dynamics. Approaches, such as metadynamics,[80] are a possible route for biasing MD simulations to efficiently explore the phase space (characterised by the collective variables) of a system allowing the bias to be assessed. Still such approaches are more mature in the area of MC simulation, which may provide further motivation toward coupled MC–MD simulations.

The coupling of MD with classical density functional theory (DFT) can be viewed as an embedded method, since information obtained from the MD simulation is communicated and analysed by using the classical DFT level of theory.[81–83] Classical DFT methods are dedicated to acquiring free energy expressions that are suitable for describing the characteristics of a system. Apart from the ideal free energy term, those expressions depend on the system, and are different for polymer, colloids, *etc.* Then, the equilibrium density distribution is self-consistently obtained through an iterative procedure that aims at minimising the free energy. The accuracy of the theoretical assumptions and the ability to provide analytical expressions for the same will determine the outcome of the DFT framework. In the case of the MD–DFT approach, one does not need to self-consistently solve the equations to obtain the density of the system at each grid cell. The detailed density distribution based on the particles' position is provided by the MD simulation and the DFT can be used to determine the different free energy components and their relative contribution to the free energy, which is often important for identifying key physical aspects of the system. A recent example of such an approach is the application of the method to identify the free energy term that mostly contributes to the rugotaxis motion of droplets on wavy substrates.[83] Another similar example of this kind of coupling, the reference interaction site model (RISM) can be coupled with MD or MC simulations, thus avoiding the necessity of iteratively solving the RISM equations, as has been shown in the calculation of solvation free energies of several small molecules.[84] In this kind of coupling, parts of the theory that are difficult to obtain analytically, can be provided as data to the different theories, as, for example in the case of MD–DFT coupling. This aspect is important for an accurate theoretical description of a system, but, also, to validate and improve the theory. In this kind of methods, MD and MC are equivalent in providing the necessary data for the coupling.

In another form of coupling, one of the methods can be at the molecular scale to readily include the molecular-level detail of the system and the other can address the mesoscale description of the fluid flow. Lattice Boltzmann (LB) is often identified as one such mesoscale method, although as it is often tuned to reproduce CFD style behaviour, so is perhaps closer to a continuum method. The LB origins in the Boltzmann equation still qualify it as somewhat more fundamental than CFD, opening up potential coupling approaches using the single particle distribution functions which are not possible using continuum models. Coupling examples using MD–LB allows for exploiting the ability of MD to deal with the simulation of molecules, which is important to describe the molecule–molecule interaction, but the same time also allows for a hydrodynamics-based description of the system.[85] Coupling of LB with MC has not been reported in the literature to the best of our knowledge. Also, LB can be coupled with particle-based models through Euler–Lagrange approaches, and various such examples already exist in the literature.[86] Variation on these LB methods[87] are often inspired by method previous developed in fluid dynamics, while various approaches can be considered for the particles, such as the discrete element method (DEM).[88] We will not expand here our discussion on all possible particle-based models available in the literature, since this clearly goes beyond the scope. Coupling of LB with MD offers advantages as both methods aim at modelling motion of fluids and are both massively parallelised and suitable for a range of diverse system geometries. The coupling to the LB equations can take place through an additional local external force to the equations and interpolation protocols, while at the same time the fluid also acts as a heat

bath for the MD particles. The approach has been demonstrated for complex fluids,[85] and recently for MD particles interacting via the MARTINI force-field.[89] Future directions in this area of coupling may include the incorporation of long-range potentials and devising new interpolation schemes for the coupling of the LB and MD domains. This might include developments on the theoretical descriptions as well as technical aspects related to the linking of lattice and off-lattice simulation models.

The extension to the simulation of biological molecules is particularly attractive for simulating solvent adequately far away from the biological molecule that we are interested to study.[90] When this type of coupling is also combined with different simulation box geometries can probably further minimise the computational resources required to simulate the solvent surrounding a biomolecule, as is commonly done in the area of biophysics, for example, for simulating proteins in solvents.

Finally, the coupling of molecular-scale models may include a variety of different particle-based models, including mesoscale models, such as dissipative particle dynamics methods (DPD). These mesoscopic models can sit as a coupling buffer between atomistic and continuum hydrodynamics.[91]

1.4 Coupling Continuum to Continuum

In the more general category of coupling in computational fluid dynamics, one can add the techniques used to add particles to continuum flows or modelling of fluid–solid interactions combining different approaches, *e.g.* finite element Analysis (FEA) with CFD. We could also consider modelling fluid in different reference frames with the moving fluid considered as a particle. This is commonly known as Euler–Lagrangian simulation approach. There are a number of different models suitable for simulating dispersed phases (*e.g.* colloids, droplets, bubbles, sand) in continuum flows, *i.e.* two-phase or more generally multiphase flows. Rather more common in the literature are studies that deal with the coupling of FEM with DEM[92] for investigating various phenomena of particles in flows, including heat transfer processes. An alternative is the Euler–Euler approach for simulating such systems., with multiphase effects taken into account in the fluids properties and through closure relations. In contrast, in the case of Euler–Lagrangian schemes, the continuous medium can be modelled by the continuum equations (*e.g.* momentum equation), while separate equations dictate the motion of the particles (Lagrangian approach), for example, Newton's equation with interactions between the particles. Coupling the two systems of equations is the goal of this approach with various options for treating the particles being available. An example here from recent work is the simulation of cloud formation.[93] In this case, 'particles' can even refer to surfactant-laden droplets with different properties, which can even change during the simulation as a result of droplet coalescence. Moreover, the model incorporates effects that arise from the reduction of surface tension due to the presence of surfactants by adopting a statistical physics (stochastic) approach for droplet processes (*e.g.* coalescence) based on the superdroplet method.[94] This indicates the variety of possibilities that can be used for the particle models in an Euler–Lagrangian approach, including the

coupling of ideas between computational fluid dynamics and statistical physics, which significantly extends the range of applications even when the approach is solely applied in the macroscale domain itself. Euler–Lagrangian models constitute a very active field of research in computational fluid dynamics, which may benefit from some of the techniques described in Sec. 2. The application of a particle-based mesoscale method, *i.e.* smoothed-particle hydrodynamics (SPH) with a continuum approach, *i.e.* finite element method (FEM) has also been reported in the literature.[95] Further work and exchange between the particle- and the continuum-simulation communities may enable the coupling of continuum models with a range of particle-based approaches towards novel applications of multiscale simulation.

2 Coupling Molecular to Continuum

Most of the focus in fluids dynamics relates to the motion of fluids and particularly on the interactions at the interfaces.[83,96–99] These interfaces can be between a solid and a liquid, or where two different fluids meet such as a liquid–vapour coexistence[100] or between two immiscible liquids.[101] These regions typically require a detailed molecular picture due to rapid changes and complexities of the interface itself. This detail is not required in the bulk, where fluid motion will be broadly identical and well described by a continuum model. As a result, continuum–molecular coupling can be used to put molecular details only where it is needed.

2.1 Coupling Types

Broadly speaking, classical fluid coupling can be divided into three categories[102] as shown in Fig. 2. In the simplest example of Fig. 2a, MD is run to obtain parameters for computational fluids dynamics (CFD). This style of parameterisation: extracting viscosity, heat flux or other transport coefficients to use in continuum models, is the aim of non-equilibrium MD (NEMD) dating back to the start of molecular simulation.[103,104] In this type of coupling, both length and time scales are decoupled so a short small MD run, especially using periodic boundaries,[105] can be representative of long temporal and spatial scales. The required assumption is that the MD domain is representative of a larger scale, accounting for finite-size effects[106] with sufficient averaging time to ensure the validity of the ergodic hypothesis. Machine learning could be used here to store more complicated behaviour than is possible with constitutive laws, for example using Artificial Neural Networks.[107]

Embedded coupling shown in Fig 2b and described in Ref. 108, is also known as the heterogeneous multi-scale method (HMM).[109] This is used in the case where complexity is too great to be characterised by simple coefficients, so small representative molecular models are run to provide refinements to the continuum model. Typically, a state of strain is applied to the individual MD runs and the resulting stress is relayed back to the continuum solver. Such techniques, *e.g.* SLLOD,[110] are valid for one directional shear and limited cases of elongation with use of a coordinate transform.[111] This limits their applicability to simple systems and a general constraint for three dimensions is required.[112]
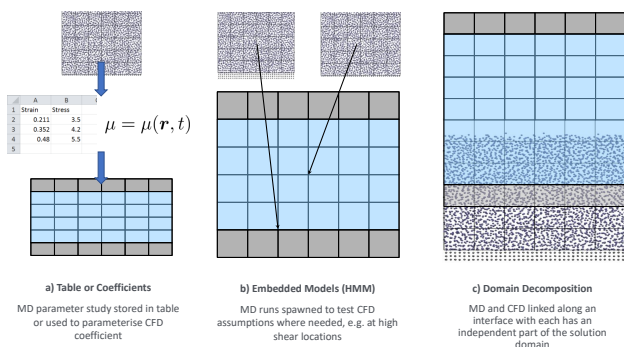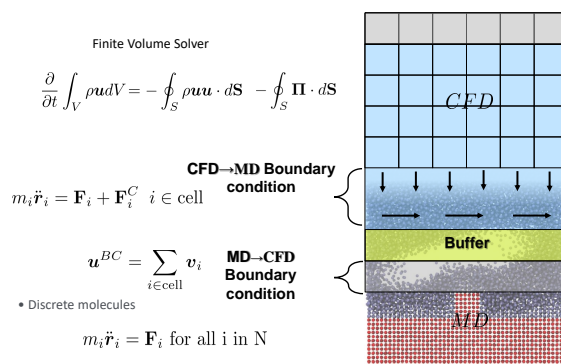
Fig. 2 Three categories of classical coupling.

Fig. 3 A domain decomposition coupling setup showing 1) the averaged region to get the CFD boundary (bottom boundary), 2) the region with an applied constraint at the top of the domain where a boundary termination force is applied to stop molecules escaping (top boundary). A buffer region is inserted for computational reasons so the constrained molecular region doesn't cause a direct feedback with the region averaged to get the boundary.

HMM has been shown to be a special case of the Mori–Zwanzig formalism.[113] An edited form of this embedded coupling was given in Ref. 114, while a detailed discussion of the limitations and shortcomings of the HMM method was reviewed in Ref. 115. Embedded coupling runs short and small representative runs so also decouples time scales from the MD and CFD system. The required assumption is that these short small runs reach a steady state, which would not change if run for longer. An example of this is the viscosity, where simulation length would only need to be sufficient for the molecule state to decorrelate. Machine learning again looks to have potential in this field. This could be built into continuum models, a kind of super resolution sub-sampling with techniques used for molecular in microscopes[116] but following similar idea of drawing small scale turbulence into larger simulations[117], where MD represents a higher-resolution region.

Finally, domain decompositional coupling shown in Fig 2c uses molecular detail in a sub-region of the wider domain. This region is then part of the large continuum simulation and the two run together with each assigned to its respective part of the domain. This technique is ideally suited to problems where molecular details are only required in a local region, such as near the wall or at the liquid–vapour interface. The continuum then becomes a technique for extending the limited spatial scale possible with molecular simulation, in that only very small regions of explicit MD detail are required. However, the two simulations are locked into the same temporal scale, as the continuum is then evolving at the same time scale as the molecular system. This should therefore be seen as a technique for accelerating MD systems, not one for including molecular detail in continuum scale problems. However, some techniques for resolving this timescale discrepancy do exist.[118,119] The earliest of these was in the work of Hadjiconstantinou et al.[37], where a Schwartz alternating method is used. This makes use of the observation that MD systems often reach a steady state quickly for given driving fluxes. This quickly converging MD system is then iterated with the continuum to obtain a pseudo-steady solution, which satisfies both. This technique has been used in Bugel et al.[47] to coupled interfaces. In this way, the MD systems can be run for short times to provide dynamics equivalent to a much longer time step.

Given the limitations of domain decomposition style coupling to the molecular time and length scale, it is reasonable to question why it is worth developing this technique. Domain decomposition is a technique to accelerate molecular simulation, by expanding the spatial domain that can be simulated using the cheaper CFD model. It is therefore not a technique which can be used to build molecular detail into CFD, at least in its current form, given the time-scale separation. The applications areas for this are therefore where MD is essential: the high pressures and strain rates of Tribology; the initial nucleation of boiling; the chemical reactions at an interface and the fundamental understanding of wall–fluid interaction, where direct numerical simulation might be applicable. Such coupling is the only possible approach in many applications where the continuum assumption or empirically derived constitutive laws fundamentally fail. The widespread utility of both classical and quantum modelling in materials science shows the potential utility of these non-continuum models. The promise of the technique for materials justifies the investment to solve these theoretical problems in fluids, and domain decomposition represents the ideal test bed to develop these solutions. Using the ideas of adaptive grid refinement, a domain decomposition could be imagined to provide insight for just the scales and times it is needed, before being switched off to allow longer time and length scales.

2.2 Introduction to Domain Decomposition

The anatomy of a domain decomposition coupling is shown in Fig. 3. This requires three features, including 1) a region which is averaged to provide a boundary condition to the continuum solver, 2) a constrained region where the fluid is driven to agree with the continuum flow-field and 3) some method of bounding the MD region at the top, either using a boundary force, a buffer of molecules, or an open boundary where molecules can be inserted.

The history of domain decomposition coupling for fluid dynamics starts with O'Connell and Thompson[31] in 1995. Despite an initial flurry of interest, work on the theoretical framework, especially the constraint forces, largely stopped with the work of

Flekkøy et al.[56] and has since focused on development of molecular insertion.[9] In comparison, the solid mechanics community has seen extensive research into the theoretical underpinning of atomistic–continuum coupling, traced back to the first papers in the 1970s.[120] This has led to a wide range of different solid coupling methodologies such as the quasicontinuum, CLS method, the FEAt, the fully non-local QC (QC-FNL) method and the CADD method, all summarised and compared in.Curtin and Miller[120] Solid mechanics typically uses the finite element form of the continuum equations, which has a clear mathematical link to the continuum equations of motion.

In solids, lattice deformations are often small so the Cauchy–Born rule can be invoked to place atoms on finite element nodes and match deformation. For fluid dynamics, such one to one linking of atoms and nodes is not possible. Instead, an Eulerian framework is commonly used, tracking the average flow of molecules as they move through a reference cell or control volume. The framework to understand these molecular averages comes from statistical mechanics, in particular NEMD.[103,104,121,122] However, the NEMD community is distinct from the coupling one, perhaps due to the more applied nature of coupled simulation. In this section, we attempt to apply two NEMD techniques to the field of coupling. In particular linking continuum and molecular equations through Irving and Kirkwood[123] and constrained dynamics using Gauss' principle of Least Constraint[103,121] to development of two of the key components of coupling: 1) coarse-graining the MD to get continuum fields and 2) the application of constraints to match MD dynamics to the CFD.

2.3 Averaging Molecular Systems

Domain decomposition coupling requires the molecular system be averaged to provide the CFD boundary condition. In the literature, coupled boundary exchange is split into state coupling,[31] obtaining the velocity and scalar pressure from MD simulation, and flux coupling, which directly couples the stress tensor from the MD system.[34,57] The Navier–Stokes equation is derived from a stress tensor, making assumptions about isotropy of the fluid, Stokes hypothesis, and incompressibility to express everything in terms of velocity and pressure. As a result, the stress-tensor approach is more general, making none of the assumptions but potentially introducing more noise into the CFD solver.[124] Although pressure measurements are said to be prohibitively noisy for coupling,[37,125] it can be shown that this depends on the definition of error and statepoint of the system.[126] As a result, the choice should be based on a method which best ensures conservation laws are valid during coupling. The finite volume (FV) method is the naturally conservative form of the continuum equations, using the equation shown in Fig. 3 expressed in terms of surface fluxes. To explore this, in this section we will express both state and flux coupling in terms of an explicitly localisation operator, which allows an equivalent to the FV form to be obtained in the MD system. This in turn provides a more rigorous expression of the averaging operation, which can be used in constrained dynamics. This operator also allows a form of stress tensor, which

improves on the virial form commonly used in the coupling literature.

Velocity (state) coupling has traditionally been expressed in the literature as obtaining the CFD boundary from a restricted sum over molecules in the MD–CFD overlapping cells,

$$\boldsymbol{u} = \sum_{i=1}^{N_I} \dot{\boldsymbol{r}}_i = \sum_{i \in \text{cell}} \dot{\boldsymbol{r}}_i, \tag{1}$$

This is a well-established binning operation in the MD literature, and as such has received minimal scrutiny in the development of coupling. There is, however, a subtlety in Eq. 1, where the second sum over N_I could equally denote molecules at a point $N_I = N_I(\boldsymbol{r},t)$ or following a collection of molecules evolving in space, i.e. $N_I = N_I(t)$. The set notation $i \in \text{cell}$ is more explicit, clearly stating only molecules located inside a cell at a given time. However, this does not tell us how these sums should behave when using the calculus, for example the time derivative of the sum of molecules $i \in \text{cell}$ must consider how the set itself changes in time. This seemingly minor consideration means the typically used constraints developed in the coupling literature are missing a critical term, as will be discussed in Sec. 2.4. In continuum fluid mechanics the relationship between following a moving collection of fluid particles and monitoring flow through a fixed region in space is given by Reynold's transport theorem, a central concept in fluid mechanics.[127] To get the molecular equivalent of Reynold's transport theorem, we formalise the localisation using a control volume integral of the Irving and Kirkwood[123] Dirac delta function.[128] The coarse-grained density and momentum in a control volume can therefore be written,

$$\int_V \rho dV = \sum_{i=1}^{N} m_i \vartheta_i = \Delta V \rho^{MD} = M_I$$

$$\int_V \rho \boldsymbol{u} dV = \sum_{i=1}^{N} m_i \dot{\boldsymbol{r}} \vartheta_i = \Delta V [\rho \boldsymbol{u}]^{MD} \tag{2}$$

where ϑ_i is zero outside a given volume and one inside, a function comprised from the product of Heaviside functions to select molecules inside the Heavisides. In the cuboidal case $\vartheta_i = \Lambda_{xi}\Lambda_{yi}\Lambda_{zi}$ where $\Lambda_{\alpha i} = H(\alpha^+ - \alpha_i) - H(\alpha^- - \alpha_i)$ and $\alpha \in \{x,y,z\}$. The cuboid has volume ΔV which is between the limits denoted by superscript $+$ and $-$, and can be made to correspond to an identical sized CFD region. The notation for the average density ρ^{MD} and momentum $[\rho \boldsymbol{u}]^{MD}$ inside the volume V is introduced and so the average control volume velocity can be defined as $\boldsymbol{u}^{MD} = [\rho \boldsymbol{u}]^{MD}/\rho^{MD}$. This has the advantage that the ϑ_i function takes care of localisation during mathematical operations. It is for this reason that taking the time evolution of Eq. (2) yields the molecular version of Reynold's transport theorem.[128] The molecular equations of Eq. (2) are expressed in the same form as the mass and momentum used in the finite volume (FV) method. The FV form is most natural for CFD simulation, owing to the conservative nature and ease of meshing for arbitrary geometry.[129]

Explicit localisation can also be used to derive a local stress tensor, to be used in flux coupling. Here, the volume average (VA) form of pressure is given by an integral of the Irving and

Kirkwood [123] stress tensor,

$$\int_V \boldsymbol{P}(\boldsymbol{r},t)dV = \overset{VA}{\mathrm{P}}\Delta V = \sum_{i=1}^N m_i \dot{\boldsymbol{r}}_i \dot{\boldsymbol{r}}_i \vartheta_i + \sum_{i,j}^N \boldsymbol{f}_{ij}\boldsymbol{r}_{ij}\ell_{ij}, \qquad (3)$$

and the ℓ_{ij} function takes the length of inter-molecular interaction inside a volume of size ΔV. For simplicity of presentation, this work doesn't separate the convective term, $i.e.$ we do not do the usual decomposition $\sum m_i \dot{\boldsymbol{r}}_i \dot{\boldsymbol{r}}_i = \rho \boldsymbol{u}\boldsymbol{u} + \sum m_i \boldsymbol{v}_i \boldsymbol{v}_i$ where $v_i = \dot{r}_i - \boldsymbol{u}$. We have also assumed a linear path of interactions between molecules [130] to avoid any ambiguity in the definition of pressure. [131] This VA pressure of Eq. (3) appears similar to the virial pressure,

$$\overset{Virial}{\mathrm{P}}\Delta V = \sum_{i=1}^N m_i \dot{\boldsymbol{r}}_i \dot{\boldsymbol{r}}_i \vartheta_i + \sum_{i,j}^N \boldsymbol{f}_{ij}\boldsymbol{r}_{ij}\vartheta_i. \qquad (4)$$

However, the pressure of Eq. (3) satisfies momentum conservation near a wall, while the virial pressure does not. [132] This is because the virial pressure assumes a homogenous system, representing a truncation to the first term in an expansion of Eq. 3. [103] Using the virial in a heterogenous MD system is known to give spurious pressure peaks near an interface. [133] Despite this error, the virial pressure is the default in two widely used open-source codes, LAMMPS and GROMACS, at the time of writing [132] and has been widely used in the coupling literature. As coupled simulations are heterogenous by construction, using the virial pressure for coupled simulations will very likely be incorrect.

The VA form is an improvement on the virial pressure, but the most natural framework for fluid dynamics is the control volume, or finite volume (FV) form, where conservation is ensured as fluxes leaving one cell are exactly equal to the fluxes into a connected cell. For a CFD solver in FV form, the boundary condition is therefore required to be a flux. In the coupling literature this virial pressure is dotted with the surface normal $\overset{Virial}{\mathrm{P}}\cdot\mathbf{n}$, to get it as a surface flux. Often the pressure uses an interpolation operation with the adjacent continuum cell to get this pressure at the location of the cells surface. [40] However, a formal version of surface flux already exists in the NEMD literature, known as the Method of Planes (MOP) pressure. [133] This is obtained from the flow of momentum carried by molecules over a given surface, for example take the x^+ surface, and the intermolecular forces acting over that surface

$$\overset{MOP}{\mathrm{P}}_{x^+} = \overset{MOP}{\mathrm{P}}{}^K_{x^+} + \overset{MOP}{\mathrm{P}}{}^C_{x^+} \qquad (5)$$

with the dashes defining surface crossings following the notation from the literature. [56]

$$\overset{MOP}{\mathrm{P}}{}^K_{x^+}\Delta A_{x^+} = \frac{1}{\Delta t}\sum_{i=1}^N m_i \dot{\boldsymbol{r}}_i \dot{x}_i dS(x_i^t, x_i^{t+\Delta t}) \equiv \sum_{i'}^{N_{x^+}} m_{i'}\dot{\boldsymbol{r}}_{i'} \qquad (6)$$

$$\overset{MOP}{\mathrm{P}}{}^C_{x^+}\Delta A_{x^+} = \sum_{i=1}^N \sum_{j\neq i}^N \boldsymbol{f}_{ij} dS(x_i, x_j) \equiv \sum_{ij'}^{N_{x^+}} \boldsymbol{f}_{ij'} \qquad (7)$$

These surfaces crossings are exactly defined in terms of rigorous mathematical functions obtained from derivatives of ϑ_i. [128,134]

Here, the crossing function is non-zero only when a molecule is crossing a surface of the finite volume,

$$dS(x_s, x_e) = \left[sign(x^+ - x_e) - sign(x^+ - x_s) \right]\Lambda_{yc}\Lambda_{zc} \qquad (8)$$

where x_s is the start of a straight line and x_e is the end, which can represent a molecule i evolving in time from position $x_i^t = x_i(t)$ to position $x_i^{t+\Delta t} = x_i(t + \Delta t)$ or the line of interaction between two molecules x_i and x_j. Note, we have written the kinetic term of Eq. (6) as the integral over a time step $(1/\Delta t)\int_t^{t+\Delta t}\delta(x^+ - x_i)\Lambda_{yi}\Lambda_{zi}dt$, so it is in the same form as the configurational term. The expression in Eq. (8) can be directly implemented in code, where the signum functions determine whether the particle has crossed a plane and, for cubic volumes, a trivial plane-line intersect calculation can give the position of crossing y_c and z_c. The crossings are used in Λ_{yc} and Λ_{zc}, respectively, which determine which control volume face it has crossed. More generally for complicated control volumes this is a ray-tracing problem over every bounding volume surface. [134] The importance of using crossings was recognised in Donev et $al.$ [135], who used a ray-tracing approach, essentially equivalent to the kinetic part of the pressure Eq. (6). This was used in coupling between CFD and Direct Simulation Monte Carlo (DSMC), building on earlier work. [136] Using this surface flux form here extends the same approach to dense fluid MD simulation, so includes the configurational term. The MOP form of pressure does not introduce the spurious oscillations, which plague the virial form of Eq. (4) and can be shown to be equivalent to the VA form [137] in the limiting case that the volumes thickness tends to zero.

Most importantly for coupling, the surface pressure of Eq. (5) is the only form that guarantees finite-volume style conservation [132] to machine precision in the MD system,

$$\frac{d}{dt}\sum_{n=1}^N m_n \dot{\mathbf{r}}_n \vartheta_n = \sum_{\alpha=1}^{Nsurf} \overset{MOP}{\mathrm{P}}{}_\alpha \Delta A_\alpha = \sum_{\alpha=1}^{Nsurf}\int_{A_\alpha}\boldsymbol{P}\cdot d\mathbf{A}_\alpha. \qquad (9)$$

The sum is over all surfaces of any bounding volume and the equality to the continuum form of surface flux over N_{surf} surfaces of the control volume $\sum_{\alpha=1}^{Nsurf}\int_{A_\alpha}\boldsymbol{P}\cdot d\mathbf{A}_\alpha$ follows directly from the time evolution of Eq. (2). In this way, it behaves in an identical way to the FV form used in CFD, where ensuring conservation is used to evolve the system in time. In the next section, the localised momentum and pressure presented here are used in the constrained dynamics equations to derive rigorous localised algorithms. By simplifying these we can explore the link between the various constraint equations used in the literature and provide a general framework to understand different coupling methodologies. These forms of constraint can also be expressed in terms of exactly conservative finite volumes, the form used in fluid dynamics solvers.

2.4 Constraint Force

A constraint force is a non-unique problem in which the total momentum of multiple molecules must be driven to some setpoint value. This setpoint is the momentum in the overlapping continuum cells, labelled $CFD \rightarrow MD$ in Fig. 3. We start by outlining

some methods for doing this based on Maxwell's Demon including particle velocity selection and selectively permeable membranes, before discussing blending functions inspired by two-phase models from CFD. We then move on to a presentation of the constraint algorithms, which are derived from the minimisation principles of physics. In particular, we show a term is missing from the most commonly used expression in the literature, due to a lack of explicit localisation of the form introduced in the previous section.

2.4.1 Maxwell's Demon

Hadjiconstantinou [124] applied the transfer from the continuum-to-molecular by selecting velocities from a Maxwell Boltzmann distribution,

$$f(\dot{r}) = \left(\frac{m}{2\pi k_B T} \right)^{\frac{3}{2}} exp \left(-\frac{m(\dot{r}-u)^2}{2k_B T} \right), \qquad (10)$$

for molecules located near the boundary of the domain. Here, k_B is Boltzmann's constant, u the continuum velocity, and T the continuum temperature. The molecular domain of interest is surrounded by a molecular reservoir. The molecule velocities are completely re-defined in line with the velocities of the overlapping continuum region. A Taylor series expansion to first order is used to establish the velocities and temperatures to be specified in the Maxwell Boltzmann distribution of Eq. (10). The effects on the dynamics of this 'Maxwell's Demon' approach are localised near the simulation boundary and the performance is said to compare favourably to constrained dynamics approaches. [124] The application of the Maxwell Boltzmann distribution was later found to result in slip, [125] which was reduced by replacing the Maxwell Boltzmann distribution function by a non-equilibrium distribution from the Chapman Enskog expansion or previous MD simulations. [125]

Liu *et al.* [118] introduce a control-style algorithm, which minimises the disturbance to a system and avoids applying any forces. This is motivated by the observation that any applied forces can have undesirable consequences as they add energy, have magnitudes 10^{12} times that of gravity, and assume a constant pressure difference. [118] To avoid applying forces, Liu *et al.* [118] use a selectively permeable membrane to bias flow in a certain direction. This membrane is also like Maxwell's demon, effectively reflecting certain molecules and allowing others through in a manner that ensures the required flow profile.

2.4.2 State Coupling

State coupling aims to control the state of the system, namely the density, velocity and temperature as opposed to the fluxes of these quantities such as pressure and heat flux. A set of coupling constraint equations is put forward in the original work of Markesteijn *et al.* [51] and extended in Korotkin *et al.* [44] In this approach, blending functions are used, which are inspired by two-phase flows in hydrodynamics, and share similarities with AdResS for molecular insertions (see section 2.5) and some of the cou-

pling techniques developed in the solid mechanics literature.

$$\dot{r}_i = \frac{p_i}{m_i} + s\left(\overline{u} - \frac{p_i}{m}\right) + \frac{s(1-s)\alpha}{\rho^{MD}}\phi_\rho \qquad (11a)$$

$$\dot{p}_i = (1-s)F_i + \frac{s(1-s)}{\rho^{MD}}\frac{\partial}{\partial r}\cdot\left(\alpha\frac{[\rho u]^{MD}}{\rho^{MD}}\phi_\rho + \beta\boldsymbol{\phi}_u\right). \quad (11b)$$

Here, the flux of density $\phi_\rho = \frac{\partial}{\partial r}\left(\overline{\rho} - \rho^{MD}\right)$ and flux of momenta $\boldsymbol{\phi}_u = \frac{\partial}{\partial r}\left(\overline{\rho u} - [\rho u]^{MD}\right)$ are introduced where ρ^{MD} and $[\rho u]^{MD}$ are as defined in Eq. 2 and the overbar quantities are the weighted average of continuum and MD systems, with density $\overline{\rho} = s\rho - (1-s)\rho^{MD}$ and velocity $\overline{u} = s(\rho u - (1-s)[\rho u]^{MD})/\overline{\rho}$. For the case when $s = 0$, we reclaim the MD equations, $\dot{r}_i = \dot{p}_i/m_i$ and $\dot{p}_i = \dot{F}_i$. For $s = 1$, the equations becomes, $\dot{r}_i = u$ and $\dot{p}_i = 0$, so the molecules are frozen, unaffected by intermolecular forces and all moving at the velocity of the overlapping continuum. In the gradual transitions from $s = 0$ to $s = 1$, any difference between the density and momentum in the two systems act to force the molecules in the direction of that difference, an example of $s = 0.5$ is included in the appendix.

These schemes represent quite a strict constraint, being exact velocity specification of every molecule in the continuum region. In some ways, they appear to mix state and flux coupling, but the fluxes are included to minimise the difference in density and velocity states between the two systems, chosen by trial and error from a choice of soft and hard constraints. [51] The forcing of Eq. (11a) and Eq. (11b) have the advantage of being flexible, with a blending function allowing easy application in complex geometries.

Arguably, the most physically-meaningful choice for a coupling scheme is one that is built on NEMD theory, designed to obey the variational forms of the equations of motion. These aim to control the average properties of a group of molecules in a way that minimises the departure from the original unconstrained dynamics. There is a long history of developing constraints in the NEMD literature. [103,121] These rely on the variational forms of the equations of motion, such as the principle of least action,

$$\delta A = \delta \int_{t_1}^{t_2} [\mathscr{L} + \lambda C] \, dt = 0, \qquad (12)$$

where $\mathscr{L}$ is the Lagrangian, C is some constraint applied to the system, and λ a Lagrangian multiplier derived to enforce the desired constraint. Constraints applied in this manner allow for the dynamics of the system to evolve in a physically correct manner (minimising the action) while simultaneously satisfying a prescribed constraint condition. This is of vital importance when the molecular system must evolve in a consistent manner with the continuum system. The constraint C can be either holonomic (a function of position and time only $C(r,t) = 0$), or non-holonomic (a function of position, velocity, and time, $C(r,\dot{r},t) = 0$). It is known that Eq. (12), when used in the Euler–Lagrange form, does not give the correct equations of motion for non-holonomic

constraints,[138] although some controversy exists.[*]

This controversy is important as the original work of O'Connell and Thompson[31], used an Euler–Lagrange equation with a constraint on the momentum of the MD system, see O'Connell[141] for full details. The constraint of O'Connell and Thompson[31] drives the MD system until it agrees with the continuum.

$$\overset{\text{OCT}}{C}(\dot{r},t) = M_I u_I(t) - \sum_{n=1}^{N_I(t)} m_n \dot{r}_n = 0, \qquad (13)$$

where $M_I u_I$ is the continuum momentum in cell I that overlaps the cell in the MD region (refer to Fig. 3, where this constrained region is labelled 'CFD $\rightarrow$ MD Boundary condition'). This apparently non-holonomic constraint is, in fact, semi-holonomic and can be integrated to give a holonomic constraint.[126] This semi-holonomic property means applying the constraint using the Euler–Lagrange equation[139] results in the following equations,

$$\dot{r}_i = \frac{p_i}{m_i} + \xi \left[\frac{M_I}{mN_I} u_I - \frac{1}{N_I} \sum_{n=1}^{N_I} \frac{p_n}{m} \right] \qquad (14a)$$

$$\dot{p}_i = -\frac{\partial \phi}{\partial r_i} = F_i, \qquad (14b)$$

written in Hamilton form. O'Connell and Thompson[31] introduce a tuning or relaxation coefficient ξ to allow the strength of constraint to be reduced. The term multiplied by ξ is proportional to the momentum difference between the molecular and continuum systems, a proportional control in the language of control theory. In the review of Bian and Praprotnik[9] the work of O'Connell and Thompson[31] is described as 'relaxation dynamics', and in Delgado-Buscalioni[49] as a Langevin equation. However, it is important to note the derivation in the thesis of O'Connell[141] is rigorously derived from the principle of least action, with no stochastic terms, and is mathematically and physically identical to the form given in the work of Nie et al.[58] as shown later in this section.

Despite its rigorous derivation from minimisation principles, the constraint of O'Connell and Thompson[31] is missing the localisation in space implied by a sum over N_I molecules, which we include through the ϑ function introduced in Sec. 2.3. This subtle difference has two important implications, 1) the constraint is not semi-holonomic with localisation (they depend on position) so it is no longer clear if the principle of least action is applicable and 2) the explicit localisation results in surface flux terms missing in previous derivations. This localisation can be included by rewriting the constraint of Eq. (13) in terms of ϑ_i as follows,

$$\overset{\text{CV}}{C}(r,\dot{r},t) = \sum_{n=1}^{N} m_n \dot{r}_n \vartheta_n - \int_V \rho u(t) dV = 0, \qquad (15)$$

Note the continuum is explicitly written in control volume or FV form, acknowledging the overlap between continuum and molecular must be over a finite volume in space and not a differential

point.[62,128] The constraint derived from the principle of least action with explicit localisation is then of the form,

$$\dot{r}_i = \frac{p_i}{m_i} + \frac{\vartheta_i}{M_I} \left[\sum_{n=1}^{N} p_n \vartheta_n - \int_V \rho u dV \right] \qquad (16a)$$

$$\dot{p}_i = F_i + \frac{m_{i'}}{M_I} \left[\sum_{n=1}^{N} p_n \vartheta_n - \int_V \rho u dV \right], \qquad (16b)$$

where Eq. (16b) has a flux term $m_{i'} = \sum_{\alpha=1}^{N_{surf}} m_i \delta(\alpha - x_i) \Lambda_{yi} \Lambda_{zi}$ which is only non-zero when a molecule is crossing one of the volume surfaces. Comparing Eq. (16b) to the O'Connell and Thompson[31] equation Eq. (14b) we see the flux term was missing in previous work due to the lack of explicit localisation. It is likely this omission has not been noticed because the proportional control force in Eq. (16a) removes any difference between molecular and continuum momenta, so any error from this missing flux term is corrected at each step. However, this missing term becomes essential when we consider the commonly used reformulation of O'Connell and Thompson[31] presented in the paper of Nie et al.[58] In its original form Nie et al.[58] obtained this by differentiating Eq. (14a) and combining with equation Eq. (14b) to give a single equation in the form,

$$m_i \ddot{r}_i = F_i + F_i^C \qquad (17)$$

where the constraint force is,

$$\overset{\text{NCER}}{F_i^C} = -\frac{1}{N_I} \sum_{n=1}^{N_I} F_n + \frac{Du_I}{Dt}. \qquad (18)$$

$$\approx -\frac{1}{N_I} \sum_{n=1}^{N_I} F_n + \frac{1}{\Delta t_{MD}} \left[u_I(t + \Delta t_{MD}) - \frac{1}{N_I} \sum_{n=1}^{N_I} \dot{r}_n(t) \right]. \qquad (19)$$

In combining the equations of O'Connell and Thompson[31], to get the constraint of Eq. (18), this changes the form of constraint to a differential control algorithm. Differential control aims to ensure the time evolution of both systems is the same. Such constraints typically perform poorly in MD systems, a well-known problem in the NEMD literature highlighted by the drift in Gaussian thermostats.[103] To overcome the limitations of using a differential constraint, Nie et al.[58] discretised the time derivative in a way that applies a further constraint proportional to the velocity in both systems, to get Eq. (19). This is justified by the requirement that the velocity of the cell at time t should tend to the velocity of the continuum at time $t + \Delta t_{MD}$, that is,

$$\frac{Du_I}{Dt} \approx \frac{u_I(t + \Delta t_{MD}) - u_I(t)}{\Delta t_{MD}} \approx \frac{1}{\Delta t_{MD}} \left[u_I(t + \Delta t_{MD}) - \frac{1}{N_I} \sum_{n=1}^{N_I} \dot{r}_n(t) \right]. \qquad (20)$$

The form of Eq. (19) can also be obtained directly from a leapfrog discretisation of Eqs. (14a) and (14b), as shown in the appendix, which emphasise the similarity between O'Connell and Thompson[31] and Nie et al.[58] However, the special discretisation of Eq. (20) is actually introducing a new proportional control, which

means the equation is no longer the form that would be derived from the principle of least action. The proportional term then ensures the systems agree is the same as the main part of the velocity controllers of,Borg et al. [60]

$$\overset{\text{BORG}}{\text{F}_i^C} = K_p \frac{m_i}{\Delta t} \left[\boldsymbol{u}(t + \Delta t) - \frac{1}{N_I} \sum_{n=1}^{N_I} \dot{\boldsymbol{r}}_n(t) \right], \qquad (21)$$

while the sum of forcing term $\frac{1}{mN_I} \sum_{i=1}^{N_I} \boldsymbol{F}_i$ is not essential to the functioning of Eq. (19). Despite this, later work by Yen et al. [142] proposed that the sum of the force terms be averaged in Eq. (18) over M iterations to address concerns with signal to noise ratios, applied together with the time averaged MD velocity instead of the instantaneous values in Eq. (20),

$$\frac{1}{mN_I} \sum_{i=1}^{N_I} \boldsymbol{F}_i \approx \left\langle \frac{1}{mN_I} \sum_{i=1}^{N_I} \boldsymbol{F}_i \right\rangle; \quad \frac{1}{N_I} \sum_{i=1}^{N_I} \dot{\boldsymbol{r}}_i(t) \approx \left\langle \frac{1}{N_I} \sum_{i=1}^{N_I} \dot{\boldsymbol{r}}_i(t) \right\rangle,$$

where angular brackets here denote an average over $M\Delta t$. A further extension of this averaged force model was deployed by Sun et al. [61], who applied the same force on all molecules in the overlap region. This could potentially have caused problems if the continuum profile varied sufficiently rapidly in the overlap region as this behaviour would not be captured. Borrowing the Quadratic Upstream Interpolation for Convective Kinetics (QUICK[129]) scheme from the continuum literature, the force applied was varied linearly across the overlap region to provide the required velocity profile. Similarly the temperature was controlled using a series of Langevin thermostats with set points based on the QUICK scheme. [61]

In a similar vein, Wang and He [45] re-introduced the scaling parameter $\xi(t)$ of O'Connell and Thompson [31] to the formula of Eq. (19). The ξ parameter was derived as a function of time by rearranging the constrained equation of motion and the constraint was applied gradually over many MD time steps. Superior performance for noisy simulation is reported by Sun et al. [61], Yen et al. [142], and Wang and He [45] when using averaged or scaled form of the Nie et al. [58] constraint. However, these changes represent a further departure from the equation obtained from the minimisation principles.

To derive a truly localised constraint from minimisation principles, we use Gauss' principle of least constraint as the constraint of Eq. (15) is non-holonomic,

$$\frac{\partial}{\partial \ddot{\boldsymbol{r}}_j} \left[\frac{1}{2} \sum_{i=1}^N m_i \left(\ddot{\boldsymbol{r}}_i - \frac{\boldsymbol{F}_i}{m_i} \right)^2 - \lambda C \right] = 0. \qquad (22)$$

This is because Gauss' Principle, as stated in Flannery [143] p23, is *'a true minimisation principle, [...] with the additional and powerful advantage that it can be applied to general non-holonomic constraints'*. Equation (22) minimises the local difference between forces and acceleration at every time, with any form of constraint applied every timestep. The price for this generality is the loss of energy conservation ensured by Hamilton's principle with holonomic constraints.

Applying Gauss' principle to the explicitly localised constraint

Eq. (15) to derive the constraint force, [62]

$$\overset{\text{CV}}{\text{F}_i^C} = -\frac{m_i \vartheta_i}{M_I} \left[\frac{d}{dt} \sum_{n=1}^N m_n \dot{\boldsymbol{r}}_n \vartheta_n - \frac{d}{dt} \int_V \rho \boldsymbol{u} dV \right] \qquad (23)$$

$$= -\frac{m_i \vartheta_i}{M_I} \left[\sum_{\alpha=1}^{Nsurf} \left(\sum_{n'}^{N_\alpha} m_{n'} \dot{\boldsymbol{r}}_{n'} + \sum_{nm'}^{N_\alpha} f_{nm'} \right) - \frac{d}{dt} \int_V \rho \boldsymbol{u} dV \right] \qquad (24)$$

$$= -\frac{m_i \vartheta_i}{M_I} \sum_{\alpha=1}^{Nsurf} \sum_{n'}^{N_\alpha} m_{n'} \dot{\boldsymbol{r}}_{n'} + \overset{\text{NCER}}{\text{F}_i^C} \qquad (25)$$

The first line, Eq. (23), simply states the time evolution of the molecular volume must be subtracted and replaced by the time evolution of its overlapping CFD counterpart. The momentum equation (Eq. (9)) is then used to obtain Eq. (24) in terms of surface fluxes. The final equality gives Eq. (25), to compare to the Nie et al. [58] constraint force. This is obtained by noticing two things, the first is the sum of N_I forces $\boldsymbol{F}_n$ is the same as the sum of forces over the control volume surface $\sum_{\alpha=1}^{Nsurf} \sum_{nm'}^{N_\alpha} f_{nm'} = \sum_{n=1}^{N_I} \boldsymbol{F}_n$. This is because all internal forces between molecules inside a control volume are equal and opposite, so only surface fluxes are non-zero after the summation over N_I. The second is that the time evolution of a control volume is a more precise notation for the substantial derivative. As the continuum cell *must* overlap a finite molecular volume $D\boldsymbol{u}/Dt$ must apply to a control volume so $\frac{d}{dt} \int_V \rho \boldsymbol{u} dV \equiv \frac{D\boldsymbol{u}_I}{Dt}$. Therefore, we see an additional surface flux term $\sum_{\alpha=1}^{Nsurf} \sum_{n'}^{N_\alpha} m_{n'} \dot{\boldsymbol{r}}_{n'}$ when compared to the force of Nie et al. [58]

We come to perhaps the most important result of this perspective: without this additional flux term, the differential constraint of Eq. (25) will not work. The Nie et al. [58] constraint and its derivatives are widely used, [21,45,48,55,61,145,146] so this error is significant to a wide range of coupling applications. It is worth noting, an identical form to Eq. (25) is obtained by directly combining Eqs. (16a) and (16b), see Smith et al. [62] for details. Explicit localisation is therefore vital to obtaining the correct constraint. This also changes the nature of the constraint, the CFD and MD systems must agree as time evolves. As a result, the constraint becomes iterative in order to ensure the applied force gives the correct momentum at the next timestep.

Implementation of Eq. (25) requires iteration to ensure fluxes are accounted for during the application of the constraint. The fluxes are the surface crossings (molecules carrying momentum into and out of a volume) which are added to the intermolecular forces (forces acting over the volume surface). To understand this, consider the process shown graphically in Fig. 4a for the case where the momentum in the CFD system is constant, so the continuum time evolution is zero i.e. $\frac{d}{dt} \int_V \rho \boldsymbol{u} dV = 0$. First, an initial guess for the evolution of molecules over the next timestep is determined from just the intermolecular forces. The molecules are projected forward and the fluxes measured over the control volume surface. The constraint force is obtained by summing both these fluxes and surface forces according to Eq. (25). This constraint force is then applied and the projected evolution of the molecules recalculated. If any molecules that previously left or entered a volume no longer do, the fluxes must be updated. This in turn changes the constraint force. Hence, a new force must

Constraint Force = −(Surface crossing + Intermolecular forces)
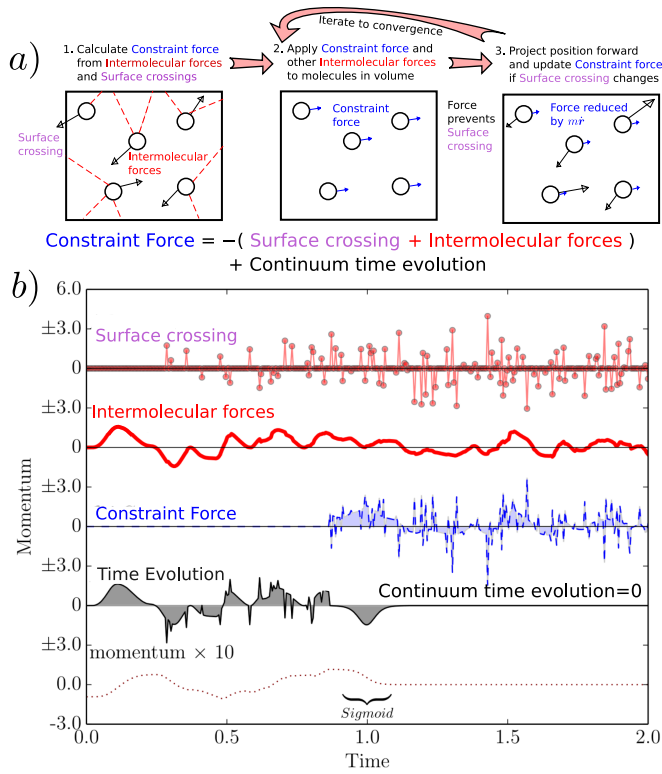+ Continuum time evolution

Fig. 4 The iterative process required for an exact constraint derived from the principle of least action or Gauss' principle is shown schematically in a), while the time evolving results for a control volume in an MD simulation are shown in b) switched on at about time 1.0 to ensure the time evolution of the control volume is equal to zero after a signum function used to set average momentum to zero. The momentum due to surface crossings is shown on the top line, intermolecular forces crossing the surface on the next line down and the required constraint force in the middle, (*i.e.* a force exactly equal to crossings and forces cancels out any momentum change). Details of the complete molecular setup are given in Smith *et al.*[144]
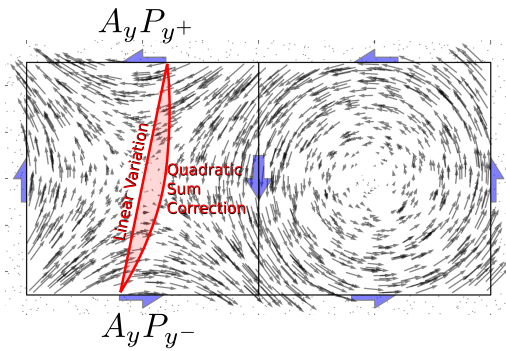

Fig. 5 A weighting function constructed to give dilatational flow in the left control volume and rotational flow on the right by choice of surface pressures, with magnitudes of $\overset{\text{Surf}}{C}_\alpha$ shown as blue arrows, where each arrow is the velocity vector at the location of a molecule. The red line shows the linear variation of force in the y direction as discussed in the text while the parabolic addition is chosen to ensure the sum of forces on all molecules obeys the required total momentum change, in this case, the total momentum change in both volumes is zero despite these spatial variations.

be calculated and this process iterated until a constraint force is consistent with the surface crossings it causes. Usually, the process takes a few iterations, even with a 3D grid of adjacent volumes each iterating their own constraint force and fluxes. The resulting constraint force is shown in Fig. 4*b*, where this force is constructed each timestep to ensure all momentum change due to fluxes over the volume surface are cancelled out. The constraint is turned on just before time $t = 1.0$ (simulation units) using a sigmoid function to guide the constrained volume to a constant momentum value of $\int_V \rho\boldsymbol{u}dV = 0$. After the constraint is applied, the momentum stays exactly at zero, the time derivative of momentum in the volume is kept at zero by the differential constraint adding a force equal to flux and surface force each time. Note that intermolecular forces are not changed and each molecule has its own momentum, the constraint only acts to ensure the total for the volume is tweaked to compensate for any surface fluxes or forces that could change the momentum inside.

Part of the reason the Nie *et al.*[58] constraint is widely used is its simplicity and robustness; at its core it is just an applied force proportional to velocity difference. The true form from the variational principles should be a differential constraint, which requires tracking of all surface fluxes and iteration. Applying such a constraint is more complex, but it is essential to apply a minimal constraint consistent with the underlying physics.

2.4.3 Flux Coupling

The importance of including fluxes naturally brings us to flux coupling. The first paper on flux coupling by Flekkøy *et al.*[34] involved introducing a flux of molecules at a rate of $\dot{N} = dN/dt$ into the molecular domain to ensure mass conservation. With molecular actively introduced, the flux is therefore easily controlled by choosing the momentum of the molecules inserted, $m\dot{N}\langle\dot{\boldsymbol{r}}'\rangle$. The velocities $\dot{\boldsymbol{r}}'$ are chosen randomly from a Maxwell Boltzmann distribution with mean value based on the continuum velocity $\boldsymbol{u}$.

Momentum conservation is ensured by constructing an applied force $\overset{\text{FWF}}{F_i^C}$ to add up to the pressure minus this momentum flux, so the resulting constraint force is then of the form,

$$\overset{\text{FWF}}{F_i^C} = \frac{g(y_i)}{\sum_i g(y_i)}\left[A\boldsymbol{P}\cdot\boldsymbol{n} - \sum_{n'} m_{n'}\dot{\boldsymbol{r}}_{n'} \right]. \qquad (26)$$

Here $g(\boldsymbol{y}_i)$ is a weighting with an arbitrary function form based on distance from the top of the domain. The flux term appearing in Eq. (26) from Flekkøy *et al.*[34] appears to be equal to the molecular insertion, $\sum_{n'} m_{n'}\dot{\boldsymbol{r}}_{n'} = m\dot{N}\langle\dot{\boldsymbol{r}}'\rangle$, although more generally this could be any molecule entering the region where the constraint is applied.

Delgado-Buscalioni and Coveney[147] extended this model by introducing an energy-based flux for the purpose of simulating unsteady flow. The weighting function was set to unity, $g(\boldsymbol{y}_i) = 1$, so that the applied force was the same for all molecules to allow easier control on the energy added as external work done becomes, $\sum F_i^C v_i = F^C \cdot \boldsymbol{u}$. The correct energy flux is ensured by inserting molecules with the appropriate kinetic energy from the Maxwell Boltzmann distribution and at a location that matches the required potential energy. Finding the required energy for

molecular insertions is a complicated aspect of coupling, and is discussed in Section 2.5. The conduction (as a temperature gradient) is matched to the continuum using a series of thermostats.

Flekkøy, Delgado-Buscalioni and Coveney[56] later reformulated this flux constraint to include a fluctuating part to control the energy addition directly,

$$\overset{\text{FDC}}{F_i^C} = \overset{\text{FWF}}{F_i^C} + F^{C\prime}. \qquad (27)$$

The constant part, $\overset{\text{FWF}}{F_i^C}$, is identical to Eq. (26) with weighting function equal to unity while the fluctuating term, $F^{C\prime}$, adds no net momentum, instead providing only energy,

$$F^{C\prime} = \frac{v_i}{\sum_{i=1}^{N_I} v_i^2} \left(\mathscr{E}A - \sum_{i\prime} \varepsilon_{i\prime} - \overset{\text{FWF}}{F_i^C} \cdot u \right). \qquad (28)$$

The magnitude of fluctuating force applied to each particle is based on the particles thermal energy, *i.e.* minus streaming term $v_i = \dot{r}_i - u$. The proposed force is said to be derived with the aim of ensuring a reversible force, one that adds no energy and ensures the probability distribution $f^{eq} = exp(-k_B \mathscr{H}/T)/Z$ is preserved at every time step, where Z is the partition function, $\mathscr{H}$ the Hamiltonian, and k_B is Boltzmann's constant. Later work by the same group,[41,42] replaced the continuum solver with the equations of fluctuating hydrodynamics.[148] These stochastic equations add an extra noise term to retain the small scale fluctuations in the continuum solver. The noise term is generated using a Wiener process and was tuned to satisfy the fluctuation–dissipation theorem. This allows molecular fluctuations to be preserved in the continuum part of the solver. These flux coupling developments are summarised in a review by Delgado-Buscalioni[49].

We can show the link between state and flux coupling, and, at the same time, show a direct derivation of flux coupling starting from Gauss' principle of least constraint. Recognising the continuum time evolution can be written in terms of surface fluxes over N_{surf} surfaces $\frac{d}{dt} \int_V \rho u dV = \sum_{\alpha=1}^{Nsurf} \int_{A_\alpha} P \cdot dA_\alpha$, we obtain from Eq. (24),

$$\overset{\text{CV}}{F_i^C} = \frac{m_i \vartheta_i}{M_I} \sum_{\alpha=1}^{Nsurf} \underbrace{\left[\int_{A_\alpha} P \cdot dA_\alpha - \sum_{n\prime}^{N_\alpha} m_{n\prime} \dot{r}_{n\prime} - \sum_{nm\prime}^{N_\alpha} f_{nm\prime} \right]}_{\overset{\text{Surf}}{C}_\alpha}. \qquad (29)$$

We introduce the notation $\overset{\text{Surf}}{C}_\alpha$ to highlight this is in the form of a constraint minimising the difference between the continuum and molecular pressures on a surface α. It is instructive to compare to the flux form of Flekkøy et al.[34] as shown in Eq. (26), chosen with the arbitrary weighting function as $g(r) = m_i \vartheta_i$ and noting $M_I = \sum_{i=1}^N m_i \vartheta_i$. As the constraint of Eq. (29) is derived for a control volume, it requires the sum of fluxes over all the surfaces of that volume (6 for a cuboid) in order to constrain the momentum inside that volume. To understand this in terms of the momentum constraint of Eq. (26), we consider the typical geometry of application used by Flekkøy et al.[34 56] As flux constraints are applied to a buffer of molecules terminating with an open boundary to a vacuum at the domain top, no intermolecular forces would

exist on the top surface y^+ and insertion is used to ensure the required momentum agrees between continuum and molecular. As a result, the momentum agreement on the top surface y^+ would be automatically ensured so does not appear in the constraint equations. Assuming periodic boundaries in the other directions, fluxes on connected faces x^+ to x^- and z^+ to z^- would cancel. As a result, only fluxes on the bottom surface need to be considered in the applied force to ensure momentum control of the volume,

$$\overset{\text{CV}}{F_i^C} = \overset{\text{FWF}}{F_i^C} - \frac{m_i \vartheta_i}{M_I} \sum_{nm\prime}^{N_{y^-}} f_{nm\prime}. \qquad (30)$$

For this particular geometry, the form of flux constraint from Flekkøy et al.[34] can be considered to be identical except for an additional intermolecular force term $f_{nm\prime}$. It is natural to ask why this additional term is not essential for flux based coupling to work successfully, as shown by various publications.[34,39–41,49,54,56] It is possible the impact of this missing intermolecular force term requires a correction, as used in Delgado-Buscalioni[49] applied to the whole volume in order to ensure conservation between CFD and MD. It is also possible this term, which depends on molecular configuration, is zero on average even for cases of strong flows. Most likely is that the form of constraint in $\overset{\text{FWF}}{F_i^C}$ has a feedback structure, so any difference between molecular momentum flux and continuum pressure is applied as a force to drive the flow (ensuring they agree). However, if an exact control on the momentum is required, or an application needs constraint in a region which is not the entire top of the simulation, then every single force and flux must be accounted for with iteration as described in Fig. 4 applied.

We have not considered the energy control introduced in Eq. (28). As the force in Eq. (29) is derived from Gauss' principle with a non-holonomic constraint, it necessarily adds energy to the system. In the limit of zero volume size, it can be shown that Eq. (29) adds the same energy to the system as the SLLOD equations of motion, important as SLLOD was derived to ensure, among other considerations, that the correct work is done on the MD system. More generally, we can ask if a momentum constraint force should add additional energy to the MD? Coupling to a CFD solver puts that continuum domain outside of the MD domain, so a coupling constraint would be expected to do work on the MD system in order to drive it. The non-holonomic nature of the constraint supports the conclusion, *i.e.* a local control of momentum as required for coupling, makes energy addition inevitable. If the continuum problem requires coupling of the energy equation, then energy control will be needed at the interface. The added constraint of Eq. (28) used in Flekkøy et al.[56] aims to control both stress heat and energy flux. There is no reason this could not be included in the extended control volume approach discussed here, provided care is taken to ensure momentum control is respected. This could be built in as an additional constraint on energy added to Gauss' principle.

This section has shown the sum of fluxes over all surfaces of a volume, with iteration, is required to enforce the correctly localised momentum constraint derived from Gauss' principle. For the specific geometry of a single constrained region at the top of

Variation Principles

Principle Least Action

$$\delta A = \delta \int_{t_1}^{t_2} [\mathcal{L} + \lambda C]\, dt = 0$$

Constraint $C^{CV}(r, \dot{r}, t)$

$$\dot{r}_i = \frac{p_i}{m_i} + \frac{\vartheta_i}{M_I}\left[\sum_{n=1}^{N} p_n \vartheta_n - \int_V \rho u\, dV\right]$$
$$\dot{p}_i = F_i + \frac{m_{i'}}{M_I}\left[\sum_{n=1}^{N} p_n \vartheta_n - \int_V \rho u\, dV\right]$$

Gauss Principle of Least Constraint

$$\frac{\partial}{\partial \ddot{r}_j}\left[\frac{1}{2}\sum_{i=1}^{N} m_i \left(r_i - \frac{F_i}{m_i}\right)^2 - \lambda C\right] = 0$$

Constraint $C^{CV}(r, \dot{r}, t)$

Smith et al (2015)

$$\overset{\text{CV}}{F_i^C} = -\frac{\vartheta_i}{M_I}\left[\frac{d}{dt}\sum_{n=1}^{N} m_n \dot{r}_n \vartheta_n - \frac{d}{dt}\int_V \rho u\, dV\right]$$

Combine equations

Express as pressure and fluxes

Flux Forms

Flekkøy et al (2005)

$$\overset{\text{FDBC}}{F_i^C} = \overset{\text{FLEK}}{F_i^C} + \frac{v_i}{\sum_{i=1}^{N_I} v_i^2}\left(\mathcal{E}A - \sum_{i'} \epsilon_{i'} - \overset{\text{FLEK}}{F_i^C}\cdot u\right)$$

Add energy control

Flekkøy et al (2000)

$$\overset{\text{FLEK}}{F_i^C} = \frac{g(y_i)}{\sum_i g(y_i)}\left[AP\cdot n - \sum_{n'} m_{n'}\dot{r}_{n'}\right]$$

One surface Neglect forces

Flux Form

$$\overset{\text{CV}}{F_i^C} = \frac{m_i \vartheta_i}{M_I}\left[\sum_{\alpha=1}^{Nsurf}\left(\int_{A_\alpha} P\cdot d\mathbf{A}_\alpha - \sum_{n'}^{N_\alpha} m_{n'}\dot{r}_{n'} + \sum_{nm'}^{N_\alpha} f_{nm'}\right)\right]$$

Neglect surface flux

O'Connell & Thompson (1995)

$$\dot{r}_i = \frac{p_i}{m} - \xi\left[\frac{1}{N_I}\sum_{n=1}^{N_I} \frac{p_n}{m} - \frac{M_I}{mN_I}u_I\right]$$
$$\dot{p}_i = -\frac{\partial \phi}{\partial r_i} = F_i$$

Neglect $m_{i'}$ Add ξ

Combine equations

Nie, Chen, E & Robbins (2004)

$$\overset{\text{NCER}}{F_i^C} = -\frac{1}{N_I}\sum_{n=1}^{N_I} F_n + \frac{Du_I}{Dt}.$$

Special discretisation

Other Forms

Borg et al (2010)

$$\overset{\text{Borg}}{F_i^C} = \frac{K_p m_i}{\Delta t_{MD}}\left[u_I(t + \Delta t_{MD}) - \frac{1}{N_I}\sum_{n=1}^{N_I} \dot{r}_n(t)\right]$$

Discretise and combine

Proportional Constraint

$$\overset{\text{NCER}}{F_i^C} = -\frac{1}{N_I}\sum_{n=1}^{N_I} F_n + \frac{1}{\Delta t_{MD}}\left[u_I(t + \Delta t_{MD}) - \frac{1}{N_I}\sum_{n=1}^{N_I} \dot{r}_n(t)\right]$$
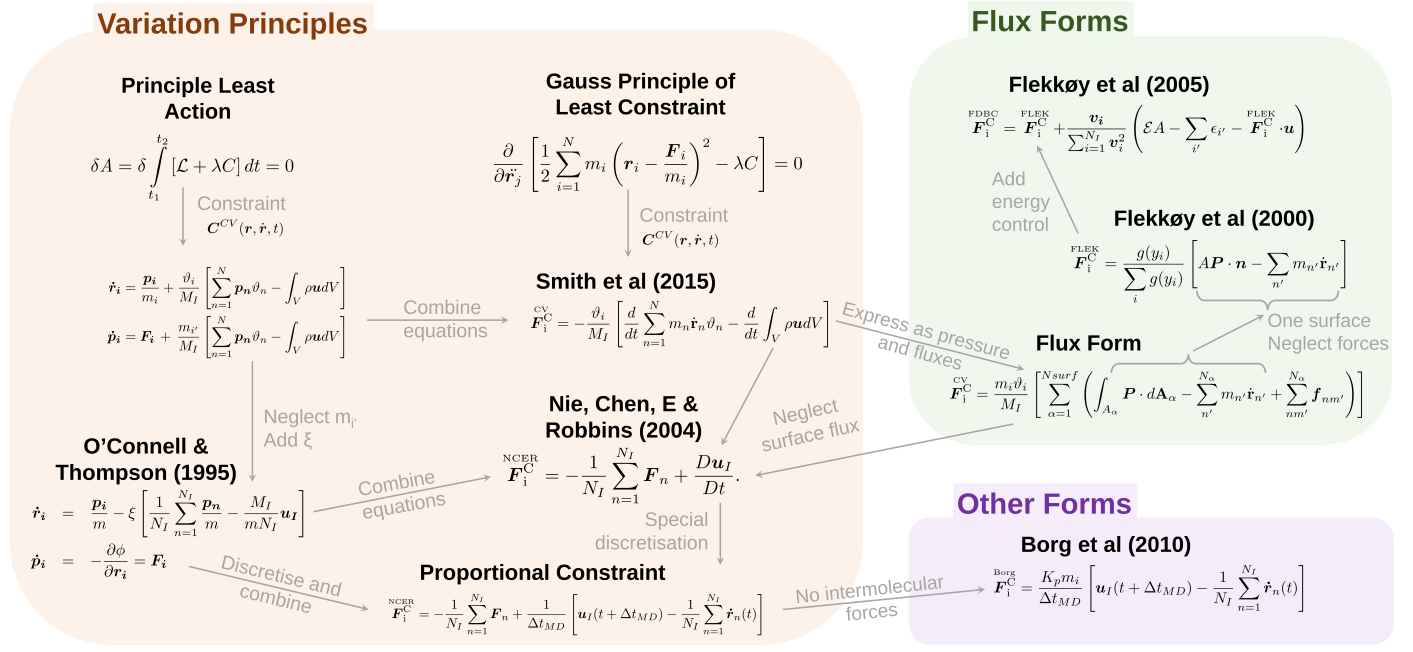
No intermolecular forces

Fig. 6 An overview of the mathematical link between the different forms of coupling constraint in the literature.

the domain, only a single surface needs to be controlled and this is equivalent to the flux coupling forms presented in the literature, as shown in Eq. (30). However, the iterative and multi-surface nature of the control volume flux constraint allows us to go beyond this single-controlled region and provide exact control over all surfaces in a grid of contiguous volumes. To do this, we use a finite element approximation to Eq. (29) in order to distribute the forces with a weighting function $g(r)$ allowing us to specify the fluxes over each surface independently. This must be designed to ensure the sum over the volume still satisfies the momentum constraint condition.[144] Perhaps the simplest form of weighting function to achieve this in a cuboidal volume is $g(r_i) = h(r_i) + \eta f(r_i)$ where the vector position denotes the product of the components in each dimension, e.g. $h(r_i) = h(x_i)h(y_i)h(z_i)$ and $f(r_i) = f(x_i)f(y_i)f(z_i)$. Using a linearly varying weight between surfaces, e.g. in x, $h(x_i) = (\overset{\text{Surf}}{C}_{x^+} - \overset{\text{Surf}}{C}_{x^-})\tilde{x}_i + \overset{\text{Surf}}{C}_{x^-}$ for $0 < \tilde{x}_i < 1$ or expressed in terms of the commonly used finite element shape functions between bottom x^- and top x^+ position, $h(x_i) = \overset{\text{Surf}}{C}_{x^+}N^+(x_i) - \overset{\text{Surf}}{C}_{x^-}N^-(x_i)$ where $N^+(x_i) = [x^+ - x_i]/\Delta x$ and $N^-(x_i) = [x_i - x^-]/\Delta x$ with $\Delta x = x^+ - x^-$.[149] The added term is constructed to be zero at the surfaces $f(x_i) = \tilde{x}_i^2 - \tilde{x}_i$ or in general coordinates, $f(x_i) = x_i^2 - x_i(x^+ + x^-) + x^+x^-$.

The η function is then chosen to ensure that $\sum_{i=1}^{N} g(r_i) = 1$, which requires,

$$\eta = \frac{1 - \sum_{n=1}^{N} h(r_n)\vartheta_n}{\sum_{n=1}^{N} f(r_n)\vartheta_n}, \tag{31}$$

Notice that the form of h could be changed to any functional form, for example a higher order element or even the radial distribution

forcing used in Werder et al.[39], and Eq. (31) would still ensure total weighting sums to unity. This constraint allows the flux over all surfaces of a control volume to be controlled, giving complicated flow-fields as shown in Fig 5. An example of using this function to varying stress control in one dimension is shown in the appendix.

In the most general case, three flux components on six surfaces can be constrained allowing 18 stresses and three momentum values to be enforced on the MD system. The distribution functions of Eq. (29) could also be chosen to control other quantities, for example aiming for a particular mass flux (e.g. $\overset{\text{Surf}}{C}_\alpha = \int_{A_\alpha} \rho u \cdot d\mathbf{A}_\alpha - \sum_{n'}^{N_\alpha} m_{n'} = 0$). This could entail controlling the linear variation of pressure so as to ensure the mass flux matches at the CFD–MD interface. Seen through this lens, the iterating required to enforce the constraint shown in Fig. 4 is analogous to the iteration used to enforce mass continuity in a CFD pressure solver by controlling pressure. Given the extensive work done on numerics and pressure solvers in the CFD community over almost seventy years, further work is certainly justified to develop such coupling framework further. Especially for multi-phase, thermal or visco-elastic models, where the coupling requirements become more complex, distribution of forces provides a method to control the MD system. More generally, the presented framework here links the main coupling approaches, as summarised in Fig. 6 and provides a potential starting point for a theoretical development to address more complex coupling requirements. It also has the potential to solve long-standing problems in embedded style coupling of applying Lees Edwards in 3D[112] by allowing full control of the stress tensor in all directions.

2.5 Molecular Insertion

Molecular insertion has been the focus of extensive research, we briefly outline the main developments here, and refer readers to Cortes-Huerto et al. [150] for a recent review. The work of O'Connell and Thompson [31] did not use particle insertion as a force is applied to stop molecules escaping, while Nie et al. [58] used the gap created by this force to make molecular insertion straight forward. In Flekkøy et al. [34] the method used to insert particles is not stated explicitly, but later papers based on the same flux coupling [147] use a steepest decent algorithm (USHER) to insert atoms at a location that gives the required potential energy. [36] For atoms and even simple molecules, this works well as it is often possible to find locations. More complex molecules, especially with long-chain are not possible to insert in this manner. One approach is to gradually increase the additional detail of these complicated molecules, forcing a region to accommodate them, as presented in the FADE algorithm. [151] The most mature method for complex molecular insertion is the adaptive resolution scheme (AdResS). In this method, one part of the system is treated at the all-atom level and another part at the coarse-grained (CG) level, thus allowing on the fly exchange of molecules between the atomic and CG levels of description through a hybrid region (Fig. 7). [77,78]
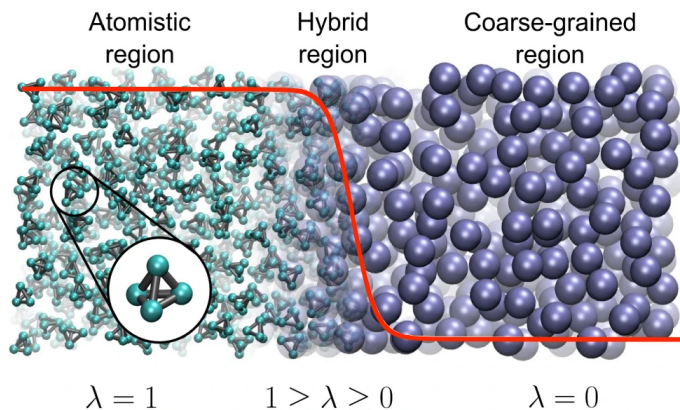

Fig. 7 Illustration of an AdResS system setup for tetrahedral molecules that can move freely between the atomistic and the CG regions through a hybrid region as indicated. Reprinted figure with permission from Ref. [152]. Copyright (2013) by the American Physical Society.

In the context of fluids, examples of the AdResS approach refer to the simulation of liquid water [152,153], which serves as a proof-of-concept for further applications. In Ref. 153, a TIP3P model was used for the all-atom representation of water and a respective CG description as well. We should however underline that the development of all-atom models for water with CG force-fields is still a very challenging aspect. For this, intensive research has led to the development of different models with each reproducing a certain range of water properties. In any case, a CG model can be obtained by the all-atom model by bottom-up approaches, for example, by matching various dynamic and structural properties (e.g. using inverse methods [154]), as well as, (thermodynamic) properties, such as pressure, etc. between the different levels of descriptions. Top-down approaches are also common, as in the case of MARTINI [155] and SAFT [156,157] force-fields. In the
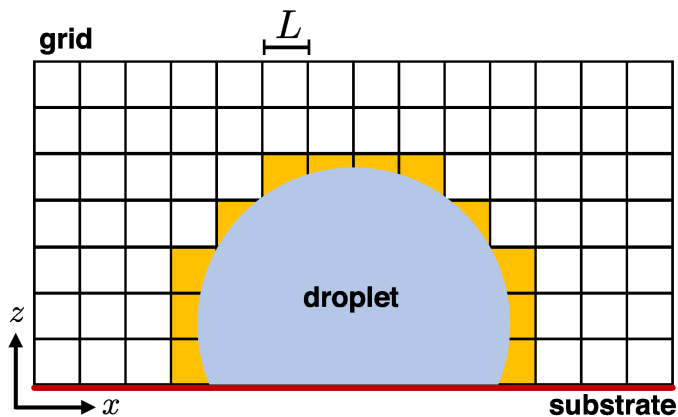

Fig. 8 Droplet on a substrate simulated via a molecular-scale MC method. The VOF in the cell is used to track the interface of the droplet, where exchange of particles takes place to investigate liquid–vapour equilibrium, condensation or evaporation phenomena. From Ref. [165].

context of AdResS, for example, a dynamic clustering algorithm that concurrently couples atomistic and CG representations has been applied in the case of a hybrid SPC/MARTINI model. [158,159] In this case, the existence of a hybrid regime can act as a glue between popular force fields, such as the SPC/E [160] and the MARTINI. [155] Finally, the link to the continuum has been demonstrated in the simulation of molecular liquids via a triple-scale simulation. [161] In this case the all-atom and CG descriptions is coupled via the AdResS scheme, while the CG level is coupled to the continuum model. Recipes to address the insertion of large molecules in the hybrid particle–continuum have been proposed, while the model seems to describe the hydrodynamics of the system. [161] The AdResS scheme has been also used with mesoscale models, such as dissipative particle dynamics (DPD), [162] where the exchange of the information between the domains is based on the open boundary method. [163,164] While there are various versions of DPD models, these models use particle descriptions, which renders the AdResS framework generally suitable for this type of coupling.

2.6 Applications

The early work on coupling typically focused on canonical flows such as the Couette and Poiseuille solutions of the Navier–Stokes equations. The flux coupling of Flekkøy et al. [34] was tested to simulate steady state Couette flow using molecular regions at the top and bottom of the domain and a continuum region between them, as well as steady state Poiseuille flow with a molecular region simulating the length of the channel (including both walls) in the streamwise direction. This flux exchange method was extended to include conservation of energy for force-driven flow over a flat wall. [35] Sun et al. [61] apply their model to Poiseuille flow with energy exchange and later to a wall of equally spaced posts. [48] The work of Yan et al. [166] represents an application of domain decomposition coupling to explore slip of a polymer melt where the near-wall region is modelled with MD and the remaining domain by CFD. They show that as shear rate drops, the computational saving increases up to two orders of magnitude. This use of coupling avoids the need for wall models and they show

the slip measures agrees very well with previous pure MD simulations. Applying coupled simulations using complex molecules for tribology applications has been discussed in Fernandez[167], while the consideration of developing slip models from coupling was given in Yang *et al.*[168] A variety of different materials with varying textures linked to varying interaction with fluids is considered in Yousefi-Nasab *et al.*[55] Heat transfer was the focus of recent coupling work,[169] while a specific application with LAMMPS and OpenFOAM is presented in Cosden and Lukes[21].

The early work of Nie *et al.*[58] also explored Couette flow and built in a post to induce a flow in the wall-normal direction. They extended this work later to lid-driven cavity flow[59] to explore the singularity present where the stationary and moving walls meet. The Nie *et al.*[58] model has been applied to a large coupled simulation by Yen *et al.*[142] They simulated a large scale Couette flow, an order of magnitude larger than that of Nie *et al.*[58] with a proportionally smaller shear rate. Start-up Couette flow was also simulated by Kamali and Kharazmi[146] with fluid flows for various micro- and nano-scale geometries studied. Delgado-Buscalioni and Coveney[147] simulated an oscillating wall (Stokes 2nd problem), which is a rare example of an unsteady problem. More extensive tests of unsteady coupling modelled include the flow of a shockwave between domains.[42] Recently, such application have been extended to practical problems such as the transmission of ultrasound.[54] More complex flow past nano-tubes in the form of cylinders was considered in Werder *et al.*[39], although only for creeping flow. It would be possible to push these simulations into the unsteady regimes, which have been shown to be possible using pure MD.[170] It is also possible to extend coupled simulation to turbulent flow,[30] where the pure MD case[171] can be seen to reproduce turbulence at the nanoscale and so a coupled model could allow quick optimisation of molecular wall effects on turbulent structures.

The blending function approach of Eqs (11a) and (11a) lends itself well to complex problems, such as the diffusion of a biomolecules in water due to Couette flow[53] and a PCV2 virus capsid in water,[52] as well an exploration of the violation of continuum laws in atomic force microscopes.[172]

In the context of multi-phase flow, the moving contact line was considered as early as 1999,[33] with later simulations of coupled droplets[145] and droplet impinging on a surface.[50] Another example uses MD simulations to generate data which is sent to a phase-field model based on the Helmholtz energy equation of state and evaluated by CFD.[173] The volume of fluid (VOF) method appears as a simple and robust approach to identify the interface between two different phases, for example between a liquid and a gas phase, due to the large density differences between the phases (Fig. 8). A scheme, such as VOF, can be combined with an off-lattice MC approach to simulate evaporation and nucleation phenomena at the molecular level.[165] The overall coupling protocol allows for the exchange of particles at the interface without the need to simulate gas molecules far from the liquid–gas interface and can be used with any force-field, be it all-atom or CG, thus allowing the simulation of a broad range of complex liquids, for example, nanofluids.[174]

3 Conclusions and Future Perspectives

A great number of coupling possibilities can be realised between currently available simulation methods. The list of available methods (and acronyms) is quite long, for example, MC, MD, DFT, VOF, FV, FEA, LB, *etc.* The possibilities are at least as many as the possible combinations of these methods and a great amount of work has been dedicated to linking the various methodologies in the most computationally efficient way and as close as possible obeying the physical laws. Here, we have not attempted to provide a detailed description of these methods, but rather provide a perspective on coupling efforts in a very focused area: MD coupled to continuum methods for fluid dynamics, in particular the popular finite volume (FV) method. Coupling time scales is important here but has been discussed in the literature.[57,63,119] Instead, the focus is on an area where less progress has been made, developing a theoretical framework for domain decomposition coupling, summarised as follow: Using an explicit localisation function based on the FV form applied to an MD system results in the form of fluxes on the surface, the MOP pressure, which avoids the well-known errors associated with the virial pressure. This description in terms of surface pressure and fluxes is consistent with the FV method used in the CFD and can be shown to be exactly conservative in an MD system. Applying this FV localisation to the derivation of a constrained dynamics algorithm results in an new surface flux term, exposing an error in the central works on coupling[31,58] and consequently all subsequent papers. The corrected constraint is differential in nature, requiring iteration to ensure the time evolution of both systems match. This general constrained form can be simplified to different well-known expressions from the literature, summarised in Fig 6, including the derivation of the flux forms from variational principles. Extending to the a finite element form gives a generalised flux coupling which can be applied to every surface of a volume in space, not just the domain top. Comprehensive control using, for example all 18 surface components of pressure, is possible and provides a template for a more general class of coupling methods. Attempts to overcome this theoretical barrier through artificial-intelligence approaches are already taking place[64] and these developments should provide a groundwork to build models on. These insights are presented in the hope that they will be a stepping stone for further work and ideas in the development of a rigourous groundwork for coupled simulation.

Conflicts of interest

There are no conflicts to declare.

Acknowledgements

Appendix

Discretising O'Connell and Thompson

A discretisation of Eqs (14a) and (14b) of O'Connell and Thompson [31] using the leapfrog scheme shows,

$$r_i(t+\Delta t) = r_i(t) + \Delta t \left(\frac{p_i(t+\Delta t/2)}{m_i} \right.$$

$$\left. +\xi \left[\frac{M_I(t)}{mN_I(t)} u_I(t+\Delta t) - \frac{1}{N_I(t)} \sum_{n=1}^{N_I(t)} \frac{p_n(t+\Delta t/2)}{m} \right] \right)$$

$$p_i(t+\Delta t/2) = p_i(t-\Delta t/2) + \Delta t F_i(t), \quad (32a)$$

these can then be combined to give,

$$\frac{r_i(t+\Delta t) - r_i(t)}{\Delta t} = \frac{p_i(t-\Delta t/2)}{m_i} + \Delta t F_i(t) - \frac{\Delta t}{N_I(t)} \sum_{n=1}^{N_I(t)} F_n(t)$$

$$+\xi \left[\frac{M_I(t)}{mN_I(t)} u_I(t+\Delta t) - \frac{1}{N_I(t)} \sum_{n=1}^{N_I(t)} \frac{p_n(t-\Delta t/2)}{m_n} \right], \tag{33}$$

where for unit mass we have $M_I = mN_I$, setting $\xi = 1$, replacing the momentum notation $p_i/m_i = \dot{r}_i$ and used the first-order backward Euler finite difference approximation $\dot{r}_i(t-\Delta t/2)/\Delta t = (r_i(t) - r_i(t-\Delta t))/(\Delta t)^2$ and second derivative $\ddot{r}_i = [r_i(t+\Delta t) - 2r_i(t) + r_i(t-\Delta t)]/(\Delta t)^2$, the form can be seen to be identical to Eq. (19) from Nie *et al.* [58] with the velocity at the half step consistent with the leapfrog scheme,

$$\ddot{r}_i = F_i(t) - \frac{1}{N_I(t)} \sum_{n=1}^{N_I(t)} F_n(t) + \frac{1}{\Delta t} \left[u_I(t+\Delta t) - \frac{1}{N_I(t)} \sum_{n=1}^{N_I(t)} \dot{r}_n(t-\Delta t/2) \right] \tag{34}$$

Note that N_I is itself a function of time and dependent on the molecular position.

Understanding the Blended Region

The constraint force of Markesteijn *et al.* [51] half way across the blending region e.g. for $s = 0.5$ is shown here,

$$\dot{r}_i = \frac{p_i}{2m_i} + \frac{\rho u - [\rho u]^{MD}}{\rho - \rho^{MD}} + \frac{\alpha}{8\rho^{MD}} \frac{\partial}{\partial r} \left(\rho - \rho^{MD} \right)$$

$$\dot{p}_i = \frac{F_i}{2} + \frac{1}{8\rho^{MD}} \frac{\partial}{\partial r} \cdot \left(\alpha \frac{[\rho u]^{MD}}{\rho^{MD}} \frac{\partial}{\partial r} \left(\rho - \rho^{MD} \right) \cdots \right.$$

$$\left. + \beta \frac{\partial}{\partial r} \left(\rho u - [\rho u]^{MD} \right) \right)$$

where the intermolecular force and momentum is half from the normal MD dynamics with the other half made up by the average of the MD and continuum system for velocity and the remaining force being a result of the gradients in differences. The gradient of the difference in density and pressure in the CFD and MD regions can be seen to apply a force driving the molecules

The flux terms ϕ_ρ and ρ_u are introduced in the derivation of

Markesteijn *et al.* [51] to give a diffusion between the two phases. These are apparently chosen as fluxes because this was found to give better behaviour than simply applying the direct difference between MD and continuum density and momenta. Later work rewrites the diffusion in terms of surface fluxes. [44] The equations are made conservative by ensuring the applied force to the MD system is equal and opposite to the continuum, where a fluctuating hydrodynamics model is used. An assumption in this derivation is the external force on the system is equal to the divergence of the pressure tensor including the fluctuating component $F^C = \nabla \cdot [P + P']$ for any system away from equilibrium. As a result, the molecular form of the pressure tensor does not appear in the equations.

An Example of Controlling Stress On 2 Surface in One Dimensional

To understand how this works, consider a force which varies only in y, we can rewrite Eq. (29) as

$$\overset{\text{Lin}}{\text{F}^C_i}(y_i) = -\overset{\text{CV}}{\text{F}^C_i} \left[\overbrace{\overset{\text{Surf}}{\text{C}}_{y^+} N^+(y_i) - \overset{\text{Surf}}{\text{C}}_{y^-} N^-(y_i)}^{\text{Linear}} \right.$$

$$\left. - \eta \underbrace{\left[y_i^2 - y_i(y^+ + y^-) + y^+ y^- \right]}_{\text{Quadratic}} \right], \tag{36}$$

so the forces applied on the top surface $\overset{\text{Surf}}{\text{C}}_{y^+}$ subtracts molecular surface pressure and adds the CFD pressure value to drive the system to have pressure $A_y P_{y^+}$, while the bottom is driven toward $A_y P_{y^-}$ with a linear variation between them as shown schematically in Fig. 5. A quadratic correction is then added, to ensure the total is as required to ensure the correct time evolution of momentum inside the volume. Figure 5 shows an example of how we can use this to induce complex flow patterns, both elongation and rotational flow in two adjacent volumes, while keeping momentum in both volumes the same *i.e.* $d/dt \sum_{i=1}^N m_i r_i \vartheta_i = 0$.

Notes and references

1 J. S. Hansen, P. J. Daivis, K. P. Travis and B. D. Todd, *Phys. Rev. E*, 2007, **76**, 041121.

2 A. Ghoufi, P. Malfreyt and D. J. Tildesley, *Chem. Soc. Rev.*, 2016, **45**, 1387–1409.

3 J. H. Snoeijer and B. Andreotti, *Ann. Rev. Fluid Mech.*, 2013, vol. 45, pp. 269–292.

4 J. C. Phillips, D. J. Hardy, J. D. C. Maia, J. E. Stone, J. V. Ribeiro, R. C. Bernardi, R. Buch, G. Fiorin, J. Hénin, W. Jiang, R. McGreevy, M. C. R. Melo, B. K. Radak, R. D. Skeel, A. Singharoy, Y. Wang, B. Roux, A. Aksimentiev, Z. Luthey-Schulten, L. V. Kalé, K. Schulten, C. Chipot and E. Tajkhorshid, *J. Chem. Phys.*, 2020, **153**, 044130.

5 S. Mapplebeck, J. Booth and D. Shalashilin, *J. Chem. Phys.*, 2021, **155**, 085101.

6 K. M. Mohamed and A. A. Mohamad, *Microfluid. Nanofluid.*, 2009, **8**, 283.

7 M. Kalweit and D. Drikakis, *IMA J. Appl. Math*, 2011, **76**, 661–671.

8 D. Drikakis and M. Frank, *Microfluid. Nanofluid.*, 2015, **19**, 1019.

9 X. Bian and M. Praprotnik, *Handbook of Materials Modeling: Applications: Current and Emerging Materials*, 2020, 2551–2571.

10 C. A. Smith and C. A. Yates, *J. R. Soc. Interface*, 2018, **15**, 20170931.

11 Z.-X. Tong, Y.-L. He and W.-Q. Tao, *Int. J. Heat Mass Transf.*, 2019, **137**, 1263–1289.

12 C. Xie and H. Li, *WIREs Comput. Mol. Sci.*, **n/a**, e1661.

13 V. R ühle, C. Junghans, A. Lukyanov, K. Kremer and D. Andrienko, *J. Chem. Theory Comput.*, 2009, **5**, 3211–3223.

14 A. H. Mazurek, L. Szeleszczuk and D. M. Pisklak, *Int. J. Mol. Sci.*, 2021, **22**, 4378.

15 A. B. Poma, M. S. Li and P. E. Theodorakis, *Phys. Chem. Chem. Phys.*, 2018, **20**, 17020–17028.

16 A. B. Poma, M. Cieplak and P. E. Theodorakis, *J. Chem. Theory Comput.*, 2017, **13**, 1366–1374.

17 M. M. Copeland, H. N. Do, L. Votapka, K. Joshi, J. Wang, R. E. Amaro and Y. Miao, *J. Phys. Chem. B*, 2022, **126**, 5810–5820.

18 K. Osaki, T. Ekimoto, T. Yamane and M. Ikeguchi, *J. Phys. Chem. B*, 2022, **126**, 6148–6158.

19 E. Shapiro, S. Rison, A. Phillips, A. Herbert and S. Emmott, *Towards 2020 Science*, Microsoft, 2006.

20 D. Henton and K. Held, *Soc. Sci. Inf.*, 2013, **52**, 539–557.

21 I. A. Cosden and J. R. Lukes, *Comput. Phys. Commun.*, 2013, **184**, 1958 – 1965.

22 M. B. Belgacem and B. Chopard, *Future Gener. Comput. Syst.*, 2017, **67**, 72–82.

23 J. Larson, R. Jacob and E. Ong, *Int. J. High Perform. Comput. Appl.*, 2005, **19**, 277–292.

24 E. Smith, D. Trevelyan, E. Ramos-Fernandez, A. Sufian, C. O'Sullivan and D. Dini, *Comput. Phys. Commun.*, 2020, **250**, 107068.

25 Y.-H. Tang, S. Kudo, X. Bian, Z. Li and G. E. Karniadakis, *J. Comp. Phys.*, 2015, **297**, 13.

26 P. Neumann, H. Flohr, R. Arora, P. Jarmatz, N. Tchipev and H.-J. Bungartz, *Comput. Phys. Commun.*, 2016, **200**, 324 – 335.

27 D. Groen, P. V. Coveney and S. J. Zasada, *2011 IEEE Seventh International Conference on e-Science Workshops (eScienceW 2011)*, 2011, **00**, 120–127.

28 J. Borgdorff, J.-L. Falcone, E. Lorenz, C. Bona-Casas, B. Chopard and A. G. Hoekstra, *J. Parallel. Distrib. Comput.*, 2013, **73**, 465 – 483.

29 D. Groen, J. Knap, P. Neumann, D. Suleimenova, L. Veen and K. Leiter, *Philos. Trans. R. Soc. Lond. A*, 2019, **377**, 20180147.

30 E. R. Smith, D. J. Trevelyan, E. Ramos-Fernandez, A. Sufian, C. O'Sullivan and D. Dini, *Comput. Phys. Commun.*, 2020, **250**, 107068.

31 S. T. O'Connell and P. A. Thompson, *Phys. Rev. E*, 1995, **52**, R5792.

32 J. Li, D. Liao and S. Yip, *Phys. Rev. E*, 1997, **57**, 7259.

33 N. G. Hadjiconstantinou, *J. Comput. Phys.*, 1999, **154**, 245.

34 E. G. Flekkøy, G. Wagner and J. Feder, *Europhys. Lett.*, 2000, **52**, 271.

35 G. Wagner, E. Flekkøy, J. Feder and T. Jossang, *Comp. Phys. Comms.*, 2002, **147**, 670.

36 R. Delgado-Buscalioni and P. Coveney, *J. Chem. Phys.*, 2003, **119**, 978.

37 N. G. Hadjiconstantinou, A. L. Garcia, M. Z. Bazant and G. He, *J. Comput. Phys.*, 2003, **187**, 274.

38 M. Praprotnik, L. D. Site and K. Kremer, *J. Chem. Phys.*, 2005, **123**, 224106.

39 T. Werder, J. H. Walther and P. Koumoutsakos, *J. Comput. Phys.*, 2005, **205**, 373.

40 G. D. Fabritiis, R. Delgado-Buscalioni and P. Coveney, *Phys. Rev. Lett.*, 2006, **97**, 134501.

41 G. D. Fabritiis, M. Serrano, R. Delgado-Buscalioni and P. Coveney, *Phys. Rev. E*, 2007, **75**, 026307.

42 R. Delgado-Buscalioni and G. D. Fabritiis, *Phys. Rev. E*, 2007, **76**, 036709.

43 E. M. Kotsalis, J. H. Walther and P. Koumoutsakos, *Phys. Rev. E*, 2007, **76**, 016709.

44 I. Korotkin, D. Nerukh, E. Tarasova, V. Farafonov and S. Karabasov, *J. Comput. Sci.*, 2016, **17**, 446–456.

45 Y. Wang and G. He, *Chem. Eng. Sci.*, 2007, **62**, 3574.

46 J. Liu, S. Chen, X. Nie and M. O. Robbins, *J. Comput. Phys.*, 2007, **227**, 279.

47 M. Bugel, G. Galliero and J. P. Caltagirone, *Microfluid. Nanofluid.*, 2011, **10**, 637.

48 J. Sun, Y. He, W. Tao, X. Yin and H. Wang, *Int. J. Numer. Meth. Engng*, 2012, **89**, 2.

49 R. Delgado-Buscalioni, *Lecture Notes in Computational Science and Engineering*, 2012, **82**, 145.

50 W.-J. Zhou, Z.-Q. Yu, Z.-Z. Li, Y.-L. He and W.-Q. Tao, *Numer. Heat Tr. A-Appl.*, 2015, **68**, 512–525.

51 A. Markesteijn, S. Karabasov, A. Scukins, D. Nerukh, V. Glotov and V. Goloviznin, *Philos. Trans. R. Soc. A*, 2014, **372**, 20130379.

52 E. V. Tarasova, I. Korotkin, V. A. Farafonov, S. A. Karabasov and D. A. Nerukh, *J. Mol. Liq.*, 2017, **245**, 109–114.

53 J. Hu, I. A. Korotkin and S. A. Karabasov, *J. Mol. Liq.*, 2019, **280**, 285–297.

54 P. Papez and M. Praprotnik, *J. Chem. Theory Comput.*, 2022, **18**, 1227–1240.

55 S. Yousefi-Nasab, J. Karimi-Sabet and J. Safdari, *Comput. Part. Mech*, 2022, 1–20.

56 E. G. Flekkøy, R. Delgado-Buscalioni and P. V. Coveney, *Phys. Rev. E*, 2005, **72**, 026703.

57 R. Delgado-Buscalioni and P. Coveney, *Phil. Trans. R. Soc. Lond.*, 2004, **362**, 1639.

58 X. B. Nie, S. Chen, E. W. N. and M. Robbins, *J. Fluid Mech.*,

2004, **500**, 55.

59 X. B. Nie, S. Chen and M. Robbins, *Phys. Fluids*, 2004, **16**, 3579.

60 M. K. Borg, G. B. Macpherson and J. M. Reese, *Molec. Sims.*, 2010, **36**, 745.

61 J. Sun, Y. He and W. Tao, *Int. J. Numer. Meth. Engng*, 2010, **81**, 207.

62 E. R. Smith, D. M. Heyes, D. Dini and T. A. Zaki, *J. Chem. Phys.*, 2015, **142**, 074110.

63 R. Delgado-Buscalioni, J. Sablić and M. Praprotnik, *The European Phys. J. Special Topics*, 2015, **224**, 2331–2349.

64 M. Raissi, P. Perdikaris and G. Karniadakis, *J. Comput. Phys.*, 2019, **378**, 686–707.

65 D. Marx and J. Hutter, *Ab Initio Molecular Dynamics: Basic Theory and Advanced Methods*, Cambridge University Press, Cambridge, 2009.

66 R. Car and M. Parrinello, *Phys. Rev. Lett.*, 1985, **55**, 2471–2474.

67 S. Izvekov and G. A. Voth, *J. Chem. Phys.*, 2005, **123**, 044505.

68 A. Vakis, V. Yastrebov, J. Scheibert, L. Nicola, D. Dini, C. Minfray, A. Almqvist, M. Paggi, S. Lee, G. Limbert, J. Molinari, G. Anciaux, R. Aghababaei, S. Echeverri Restrepo, A. Papangelo, A. Cammarata, P. Nicolini, C. Putignano, G. Carbone, S. Stupkiewicz, J. Lengiewicz, G. Costagliola, F. Bosia, R. Guarino, N. Pugno, M. Müser and M. Ciavarella, *Tribol. Int.*, 2018, **125**, 169–199.

69 A. Warshel and M. Levitt, *J. Mol. Biol.*, 1976, **103**, 227–249.

70 E. Brunk and U. Rothlisberger, *Chem. Rev.*, 2015, **115**, 6217–6263.

71 S. Dapprich, I. Komáromi, K. Byun, K. Morokuma and M. J. Frisch, *J. Mol Struct.: THEOCHEM*, 1999, **461-462**, 1–21.

72 X. Qu, P. Xu, R. Li, G. Li, L. He and X. Ren, *J. Chem. Theory Comput.*, 0, **0**, null.

73 P. Restuccia, M. Ferrario and M. C. Righi, *Comput. Mater. Sci.*, 2020, **173**, 109400.

74 J. F. Gilabert, O. Gracia Carmona, A. Hogner and V. Guallar, *J. Chem. Inf. Model*, 2020, **60**, 5529–5539.

75 Y. Chen, A. J. Schultz and J. R. Errington, *J. Phys. Chem.*, 2021, **125**, 8193–8204.

76 F. Wang and D. P. Landau, *Phys. Rev. E*, 2001, **64**, 056101.

77 M. Praprotnik, L. Delle Site and K. Kremer, *J. Chem. Phys.*, 2005, **123**, 224106.

78 M. Praprotnik, L. Delle-Site and K. Kremer, *Annu. Rev. Phys. Chem.*, 2008, **59**, 545–571.

79 M. S. Barhaghi, B. Crawford, G. Schwing, D. J. Hardy, J. E. Stone, L. Schwiebert, J. Potoff and E. Tajkhorshid, *J. Chem. Theory Comput.*, 2022, **18**, 4983–4994.

80 A. Laio and M. Parrinello, *Proc. Natl. Acad. Sci. U.S.A.*, 2002, **99**, 12562–12566.

81 A. Milchev, S. Egorov, D. Vega, K. Binder and A. Nikoubashman, *Macromolecules*, 2018, **51**, 2002–2016.

82 F. Lo Verso, L. Yelash, S. Egorov and K. Binder, *J. Chem. Phys.*, 2011, **135**, 214902.

83 P. E. Theodorakis, S. A. Egorov and A. Milchev, *EPL*, 2002, **137**, 43002.

84 H. Freedman and T. N. Truong, *Chem. Phys. Lett.*, 2003, **381**, 362–367.

85 F. Mackay, S. Ollila and C. Denniston, *Comput. Phys. Commun.*, 2013, **184**, 2021–2031.

86 O. Filippova and D. Hänel, *Comput. Fluids*, 1997, **26**, 697–712.

87 S. Liu, C. Zhang and R. B. Ghahfarokhi, *Energy Fuels*, 2021, **35**, 13535–13549.

88 R. Zhang, H.-J. Kim and P. R. Dinoy, *Appl. Sci.*, 2021, **11**, 3436.

89 X. Yu and M. Dutt, *Comput. Phys. Commun.*, 2020, **257**, 107287.

90 J. Zavadlav, J. Sablić, R. Podgornik and M. Praprotnik, *Biophys. J.*, 2018, **114**, 2352–2362.

91 R. Delgado-Buscalioni, K. Kremer and M. Praprotnik, *J. Chem. Phys.*, 2009, **131**, 244107.

92 H. Haddad, M. Guessasma and J. Fortin, *Int. J. Solids Struct.*, 2016, **81**, 203–218.

93 M. Denys, P. Deuar, Z. Che and P. E. Theodorakis, *Phys. Fluids*, 2022, **34**, 095126.

94 S. Shima, K. Kusano, A. Kawano, T. Sugiyama and S. Kawahara, *Q. J. R. Meteorol. Soc.*, 2009, **135**, 1307–1320.

95 Z. Zhang, H. Qiang and W. Gao, *Eng. Struct.*, 2011, **33**, 255–264.

96 P. E. Theodorakis, E. A. Müller, R. V. Craster and O. K. Matar, *Langmuir*, 2015, **31**, 2304–2309.

97 P. E. Theodorakis, A. Amirfazli, B. Hu and Z. Che, *Langmuir*, 2021, **37**, 4248–4255.

98 P. E. Theodorakis, S. A. Egorov and A. Milchev, *J. Chem. Phys.*, 2017, **147**, 244705.

99 R. Kajouri, P. E. Theodorakis, P. Deuar, R. Bennacer, J. Žídek, S. A. Egorov and A. Milchev, *Langmuir*, 2023, **39**, 2818–2828.

100 P. Morgado, O. Lobanova, E. A. Müller, G. Jackson, M. Almeida and E. J. Filipe, *Mol. Phys.*, 2016, **114**, 2597–2614.

101 H. Xu, T. Wang and Z. Che, *J. Colloid Interface Sci.*, 2022, **628**, 869–877.

102 E. R. Smith, P. E. Theodorakis, R. V. Craster and O. K. Matar, *Langmuir*, 2018, **34**, 12501–12518.

103 D. J. Evans and G. P. Morriss, *Statistical Mechanics of Non-Equilibrium Liquids*, Australian National University Press, Canberra, 2nd edn, 2007.

104 B. D. Todd and P. J. Daivis, *Nonequilibrium Molecular Dynamics: Theory, Algorithms and Applications*, Cambridge University Press, Cambridge, 1st edn, 2017, p. 367.

105 A. W. Lees and S. F. Edwards, *J. Phys. C: Solid State Phys.*, 1972, **5**, 1921.

106 S. I. Sandler and L. V. Woodcock, *J. Chem. Eng. Data*, 2010, **55**, 4485.

107 N. Asproulis and D. Drikakis, *Microfluid. Nanofluid.*, 2013, **15**, 559–574.

108 W. Ren, *J. Comput. Phys.*, 2007, **227**, 1353.

109 W. E, B. Engquist, X. Li, W. Ren and E. Vanden-Eijnden, *Commun. Comput. Phys.*, 2007, **2**, 367–450.

110 W. G. Hoover, C. G. Hoover and J. Petravic, *Phys. Rev. E*, 2008, **78**, 046701.

111 F. Frascoli, D. J. Searles and B. D. Todd, *Phys. Rev. E*, 2006, **73**, 046206.

112 S. Yasuda and R. Yamamoto, *Phys. Fluids.*, 2008, **20**, 113101.

113 J. R. Price, *PhD thesis*, 2018.

114 M. K. Borg, D. A. Lockerby and J. M. Reese, *J. Comput. Phys.*, 2013, **233**, 400.

115 S. Stalter, L. Yelash, N. Emamy, A. Statt, M. Hanke, M. Lukáčová-Medviďová and P. Virnau, *Comput. Phys. Commun.*, 2018, **224**, 198–208.

116 N. Liu, M. Dai, S. K. Saka and P. Yin, *Nat. Chem.*, 2019, **11**, 1001.

117 K. Fukami, K. Fukagata and K. Taira, *J. Fluid Mech.*, 2019, **870**, 106–120.

118 J. Liu, S. Y. Chen, X. B. Nie and M. O. Robbins, *Comms. Comp. Phys.*, 2008, **4**, 1279.

119 D. A. Lockerby, C. A. Duque-Daza, M. K. Borg and J. M. Reese, *J. Comput. Phys.*, 2013, **237**, 344.

120 W. A. Curtin and R. E. Miller, *Modelling Simul. Mater. Sci. Eng.*, 2003, **11**, 33.

121 W. G. Hoover, *Computational Statistical Mechanics*, Elsevier Science, Oxford, 1st edn, 1991.

122 M. E. Tuckerman, *Statistical Mechanics: Theory and Molecular Simulation*, Oxford University Press, 1st edn, 2010.

123 J. H. Irving and J. G. Kirkwood, *J. Chem. Phys.*, 1950, **18**, 817.

124 N. G. Hadjiconstantinou, *PhD thesis*, MIT (U.S.), 1998.

125 N. G. Hadjiconstantinou, *Bull. Pol. Acad. Sci.*, 2005, **53**, 335.

126 E. R. Smith, *PhD thesis*, Imperial College London, 2014.

127 M. C. Potter and D. C. Wiggert, *Mechanics of Fluids*, Brooks/Cole, California, 3rd edn, 2002.

128 E. R. Smith, D. M. Heyes, D. Dini and T. A. Zaki, *Phys. Rev. E.*, 2012, **85**, 056705.

129 C. Hirsch, *Numerical Computation of Internal and External Flows*, Elsevier, Oxford, 2nd edn, 2007.

130 J. Cormier, J. M. Rickman and T. J. Delph, *J. Appl. Phys.*, 2001, **89**, 99.

131 P. Schofield and J. R. Henderson, *Proc. R. Soc. Lond. A*, 1982, **379**, 231.

132 K. Shi, E. R. Smith, E. E. Santiso and K. E. Gubbins, *J. Chem. Phys.*, 2023, **158**, 040901.

133 B. D. Todd, D. J. Evans and P. J. Daivis, *Phys. Rev. E*, 1995, **52**, 1627.

134 E. R. Smith, *Mol. Simul.*, 2022, **48**, 57–72.

135 A. Donev, J. B. Bell, A. L. Garcia and B. J. Alder, *Multiscale Model. Simul.*, 2010, **8**, 871–911.

136 A. L. Garcia, J. B. Bell, W. Y. Crutchfield and B. J. Alder, *J. Comput. Phys.*, 1999, **154**, 134–155.

137 D. M. Heyes, E. R. Smith, D. Dini, H. A. Spikes and T. A. Zaki, *J. Chem. Phys.*, 2012, **136**, 134705.

138 E. J. Saletan and A. H. Cromer, *Am. J. Phys.*, 1970, **38**, 892.

139 H. Goldstein, C. Poole and J. Safko, *Classical Mechanics*, Addison Wesley, Boston, 3rd edn, 2002.

140 M. R. Flannery, *Am. J. Phys.*, 2005, **73**, 265.

141 S. O'Connell, *PhD thesis*, Duke Uni. (U.S.), 1995.

142 T. H. Yen, C. Y. Soong and P. Tzeng, *Microfluid. Nanofluid.*, 2007, **3**, 665.

143 M. R. Flannery, *J. Math. Phys.*, 2011, **52**, 032705.

144 E. Smith, D. Heyes, D. Dini and T. Zaki, *J. Chem. Phys.*, 2015, **142**, 074110.

145 H. Wu, K. Fichthorn and A. Borhan, *Heat Mass Transf.*, 2014, **50**, 351.

146 R. Kamali and A. Kharazmi, *Comput. Phys. Commun.*, 2013, **184**, 2316–2320.

147 R. Delgado-Buscalioni and P. Coveney, *Phys. Rev. E*, 2003, **67**, 046704.

148 L. D. Landau and E. M. Lifshitz, *Fluid Mechanics*, Pergamon Press, 1st edn, 1969.

149 O. Zienkiewicz, *The Finite Element Method: Its Basis and Fundamentals*, Elsevier Butterworth-Heinemann, Oxford, 6th edn, 2005.

150 R. Cortes-Huerto, M. Praprotnik, K. Kremer and L. Delle-Site, *Eur. Phys. J. B*, 2021, **94**, 189.

151 M. K. Borg, D. A. Lockerby and J. M. Reese, *J. Chem. Phys.*, 2014, **140**, 074110.

152 R. Potestio, S. Fritsch, P. Español, R. Delgado-Buscalioni, K. Kremer, R. Everaers and D. Donadio, *Phys. Rev. Lett.*, 2013, **110**, 108301.

153 M. Praprotnik, S. Matysiak, L. D. Site, K. Kremer and C. Clementi, *J. Phys.: Condens. Matter*, 2007, **19**, 292201.

154 D. Reith, M. Pütz and F. Müller-Plathe, *J. Comput. Chem.*, 2003, **24**, 1624–1636.

155 P. C. T. Souza, R. Alessandri, J. Barnoud, S. Thallmair, I. Faustino, F. Grünewald, I. Patmanidis, H. Abdizadeh, B. M. H. Bruininks, T. A. Wassenaar, P. C. Kroon, J. Melcr, V. Nieto, V. Corradi, H. M. Khan, J. Domański, M. Javanainen, H. Martinez-Seara, N. Reuter, R. B. Best, I. Vattulainen, L. Monticelli, X. Periole, A. H. Tieleman, D. P. de Vries and S. J. Marrink, *Nat. Methods*, 2021, 382–388.

156 E. A. Müller and G. Jackson, *Annu. Rev. Chem. Biomol. Eng.*, 2014, **5**, 405–427.

157 T. Lafitte, A. Apostolakou, C. Avendaño, A. Galindo, C. S. Adjiman, E. A. Müller and G. Jackson, *J. Chem. Phys.*, 2013, **139**, 154504.

158 J. Zavadlav, S. J. Marrink and M. Praprotnik, *J. Chem. Theory Comput.*, 2016, **12**, 4138–4145.

159 J. Zavadlav, S. J. Marrink and M. Praprotnik, *Interface Focus*, 2019, **9**, 20180075.

160 H. J. C. Berendsen, J. R. Grigera and T. P. Straatsma, *J. Phys. Chem.*, 1987, **91**, 6269–6271.

161 R. Delgado-Buscalioni, K. Kremer and M. Praprotnik, *J. Chem. Phys.*, 2008, **128**, 114110.

162 P. Papež and M. Praprotnik, *J. Chem. Theory. Comput.*, 2022,

18, 1227–1240.

163 E. G. Flekkøy, R. Delgado-Buscalioni and P. V. Coveney, *Phys. Rev. E*, 2005, **72**, 026703.

164 R. Delgado-Buscalioni, J. Sablić and M. Praprotnik, *Eur. Phys. J. Spec. Top.*, 2015, **224**, 2331–2349.

165 P. E. Theodorakis, Y. Wang, A. Chen and B. Liu, *Materials*, 2021, **14**, 2092.

166 H. J. Yan, F. H. Qin, Z. H. Wan and D. J. Sun, *Microfluid. Nanofluid.*, 2021, **25**, 1–10.

167 E. R. Fernandez, *PhD thesis*, Imperial College London, 2021.

168 J. Yang, Z. Wan, L. Wang and D. Sun, *J. Fluids Eng.*, 2018, **140**, 101101.

169 Y. Liu, L. Liu, W. Zhou and J. Wei, *J. Mol. Liq.*, 2021, **340**, 117178.

170 D. C. Rapaport, *The Art of Molecular Dynamics Simulation*, Cambridge University Press, Cambridge, 2nd edn, 2004.

171 E. R. Smith, *Phys. Fluids*, 2015, **27**, 115105.

172 F. Li, S. K. Smoukov, I. Korotkin, M. Taiji and S. Karabasov, *Langmuir*, 2023, **39**, 220–226.

173 M. Heinen, M. Hoffmann, F. Diewald, S. Seckler, K. Langenbach and J. Vrabec, *Phys. Fluids*, 2022, **34**, 042006.

174 B. Liu, S. Wang, L. Chai, G. El Achkar, A. Chen and P. E. Theodorakis, *Eur. Phys. J. Appl. Phys.*, 2020, **92**, 11101.